NAVAL POSTGRADUATE SCHOOL

MONTEREY, CALIFORNIA

THESIS

TIN AS A SHOCK-MELTING BINDER FOR REACTIVE MATERIALS

by

Owen S. Esposito

June 2020

Thesis Advisor: Joseph P. Hooper
Second Reader: Brian Mason

Approved for public release. Distribution is unlimited.

THIS PAGE INTENTIONALLY LEFT BLANK

REPORT DOCUMENTATION PAGE			*Form Approved OMB No. 0704-0188*

1. AGENCY USE ONLY *(Leave blank)*	**2. REPORT DATE** June 2020	**3. REPORT TYPE AND DATES COVERED** Master's thesis

4. TITLE AND SUBTITLE
TIN AS A SHOCK-MELTING BINDER FOR REACTIVE MATERIALS

5. FUNDING NUMBERS
RPMU9; RPMTR

6. AUTHOR(S) Owen S. Esposito

7. PERFORMING ORGANIZATION NAME(S) AND ADDRESS(ES)
Naval Postgraduate School
Monterey, CA 93943-5000

8. PERFORMING ORGANIZATION REPORT NUMBER

9. SPONSORING / MONITORING AGENCY NAME(S) AND ADDRESS(ES)
Office of Naval Research

10. SPONSORING / MONITORING AGENCY REPORT NUMBER

11. SUPPLEMENTARY NOTES The views expressed in this thesis are those of the author and do not reflect the official policy or position of the Department of Defense or the U.S. Government.

12a. DISTRIBUTION / AVAILABILITY STATEMENT
Approved for public release. Distribution is unlimited.

12b. DISTRIBUTION CODE
A

13. ABSTRACT (maximum 200 words)

Reactive material warhead cases have the potential to greatly increase ordnance lethality by the addition of metal combustion, to explosive and fragmentation effects. Efficient combustion of the reactive metal relies on adequate dispersion of fine metal debris following detonation or impact. This thesis examines the use of tin as a soft binder for cold-isostatically pressed aluminum powder. The tin can potentially shock melt under rapid loading, increasing the dispersion of the aluminum by dynamically creating liquid failure regions. Several mechanical tests, including Split-Hopkinson Pressure Bar compression and Brazilian tension tests, gas gun impact tests, and three-point bend tests, as well as scanning electron microscopy, were used to determine dynamic strength, fragmentation properties, fracture toughness, and other mechanical properties of aluminum-tin composites of varying composition. Samples with lower tin content (5–10% by volume) were highly homogeneous and had low porosity following annealing. However, from a structural standpoint the tin binder results in reductions in strength and toughness compared to a pure pressed-aluminum powder compact. Analysis of the microstructure shows that tin acts as a soft buffer, weakening mechanical properties by preventing interlocking of the aluminum particles during the compaction. The final optimized composite may be useful for enhanced blast thermobaric cases that favor metal dispersion over structural strength.

14. SUBJECT TERMS
explosives, reactive materials, fragmentation

15. NUMBER OF PAGES
93

16. PRICE CODE

17. SECURITY CLASSIFICATION OF REPORT	**18. SECURITY CLASSIFICATION OF THIS PAGE**	**19. SECURITY CLASSIFICATION OF ABSTRACT**	**20. LIMITATION OF ABSTRACT**
Unclassified	Unclassified	Unclassified	UU

NSN 7540-01-280-5500

Standard Form 298 (Rev. 2-89)
Prescribed by ANSI Std. 239-18

THIS PAGE INTENTIONALLY LEFT BLANK

Approved for public release. Distribution is unlimited.

TIN AS A SHOCK-MELTING BINDER FOR REACTIVE MATERIALS

Owen S. Esposito
Ensign, United States Navy
BS, Georgia Institute of Technology, 2019

Submitted in partial fulfillment of the
requirements for the degree of

MASTER OF SCIENCE IN APPLIED PHYSICS

from the

NAVAL POSTGRADUATE SCHOOL
June 2020

Approved by: Joseph P. Hooper
Advisor

Brian Mason
Second Reader

Kevin B. Smith
Chair, Department of Physics

THIS PAGE INTENTIONALLY LEFT BLANK

ABSTRACT

Reactive material warhead cases have the potential to greatly increase ordnance lethality by the addition of metal combustion, to explosive and fragmentation effects. Efficient combustion of the reactive metal relies on adequate dispersion of fine metal debris following detonation or impact. This thesis examines the use of tin as a soft binder for cold-isostatically pressed aluminum powder. The tin can potentially shock melt under rapid loading, increasing the dispersion of the aluminum by dynamically creating liquid failure regions. Several mechanical tests, including Split-Hopkinson Pressure Bar compression and Brazilian tension tests, gas gun impact tests, and three-point bend tests, as well as scanning electron microscopy, were used to determine dynamic strength, fragmentation properties, fracture toughness, and other mechanical properties of aluminum-tin composites of varying composition. Samples with lower tin content (5–10% by volume) were highly homogeneous and had low porosity following annealing. However, from a structural standpoint the tin binder results in reductions in strength and toughness compared to a pure pressed-aluminum powder compact. Analysis of the microstructure shows that tin acts as a soft buffer, weakening mechanical properties by preventing interlocking of the aluminum particles during the compaction. The final optimized composite may be useful for enhanced blast thermobaric cases that favor metal dispersion over structural strength.

THIS PAGE INTENTIONALLY LEFT BLANK

TABLE OF CONTENTS

I. INTRODUCTION....1

II. EXPERIMENTAL METHODOLOGY....3
A. SAMPLE PREPARATION....3
1. Mixture Preparation....3
2. Pressing of Samples....5
3. Machining/Cutting....8
4. Heat Treatment....9
B. MECHANICAL TESTING....12
1. Split-Hopkinson Pressure Bar (SHPB)....12
2. Three Point Bend....14
3. 0.5" Gas Gun....15
C. SCANNING ELECTRON MICROSCOPY....17
D. SAMPLE WARHEAD CASINGS....19

III. RESULTS AND DISCUSSION....23
A. POROSITY....23
B. MECHANICAL PROPERTIES....28
1. Tensile Strength....28
2. Compressive Strength....30
3. Fracture Toughness....32
4. Gas Gun and Fragmentation Analysis....33
C. SEM IMAGING....35

IV. CONCLUSIONS AND FUTURE WORK....45

APPENDIX A. HOPKINSON BAR TEST IMAGE SEQUENCES....47

APPENDIX B. SEM IMAGES....53

APPENDIX C. SAMPLE DATA....67

LIST OF REFERENCES....71

INITIAL DISTRIBUTION LIST....73

THIS PAGE INTENTIONALLY LEFT BLANK

LIST OF FIGURES

Figure 1. Mixture preparation materials. 4

Figure 2. Ball mill. 5

Figure 3. Sample pressing materials. 6

Figure 4. Sample mold prepared for pressing. 7

Figure 5. Cold isostatic press (CIP). 7

Figure 6. Pressed Al/Sn rod using CIP. 8

Figure 7. Cutting saw. 8

Figure 8. Samples cut from a pressed rod. 9

Figure 9. Sample dimensions. 9

Figure 10. Yamato vacuum drying oven. 10

Figure 11. Exuded tin and tin oxide on surface of samples. 11

Figure 12. Exuded tin and tin oxide on sample surface (closeup). 11

Figure 13. Small muffle furnace. 12

Figure 14. Split-Hopkinson pressure bar (SHPB) setup. Source: [4]. 13

Figure 15. Brazilian tension test configuration. 14

Figure 16. Three point bend H15 Al sample. 15

Figure 17. 0.5” Gas Gun at NPS. 15

Figure 18. 0.5” Gas Gun Test Setup. Source: [13]. 16

Figure 19. Sieves and vibration table. 17

Figure 20. Zeiss scanning electron microscope (SEM). 18

Figure 21. Mounted SEM samples. 19

Figure 22. Large batch of Al/Sn powder. 20

Figure 23. Mold for pressing warhead case. 21

Figure 24. Warhead case mold prepared for pressing. 21
Figure 25. Warhead case fractured during pressing. 22
Figure 26. Pressed warhead case. 22
Figure 27. Porosity before and after heating (all samples). 24
Figure 28. Change in porosity after heating. 25
Figure 29. Change in porosity after heating for 30 minutes at 200°C (H2 samples). 26
Figure 30. Change in porosity after heating for 120 minutes at 200°C (H2 samples). 26
Figure 31. Change in porosity after heating for 30 minutes at 200°C (H15 samples). 27
Figure 32. Change in porosity after heating for 120 minutes at 200°C (H15 samples). 28
Figure 33. Tensile strengths. 29
Figure 34. Compressive strengths. 31
Figure 35. Gas gun shot 1. 33
Figure 36. Gas gun shot 2. 33
Figure 37. Gas gun shot 3. 34
Figure 38. Fragments collected from gas gun impact. 34
Figure 39. Gas gun impact fragment distribution. 35
Figure 40. Progression of tin content for H15 samples heated for 30 minutes. 37
Figure 41. Progression of tin content for H15 samples heated for 120 minutes. 38
Figure 42. Progression of tin content for H2 samples heated for 30 minutes. 39
Figure 43. Progression of tin content for H2 samples heated for 120 minutes. 40
Figure 44. Distribution of tin in H15 (a, b) and H2 (c, d) with 5% (a, c) and 25% (b, d) Sn heated for 120 minutes. 41
Figure 45. Exuded tin and tin oxide (SED). 42

Figure 46. 50% Sn (H15 Al) heated for 5, 30, and 120 minutes. 43
Figure 47. Pure H15 heated for 30 minutes (Brazilian test). 47
Figure 48. Pure H15 heated for 120 minutes (Brazilian test). 47
Figure 49. Pure H2 heated for 30 minutes (Brazilian test). 47
Figure 50. Pure H2 heated for 120 minutes (Brazilian test). 47
Figure 51. 5% Sn (H15) heated for 30 minutes (Brazilian test). 47
Figure 52. 5% Sn (H15) heated for 120 minutes (Brazilian test). 48
Figure 53. 5% Sn (H2) heated for 30 minutes (1) (Brazilian test). 48
Figure 54. 5% Sn (H2) heated for 120 minutes (1) (Brazilian test). 48
Figure 55. 5% Sn (H2) heated for 30 minutes (2) (Brazilian test). 48
Figure 56. 5% Sn (H2) heated for 120 minutes (2) (Brazilian test). 48
Figure 57. 7.5% Sn (H15) heated for 30 minutes (Brazilian test). 49
Figure 58. 7.5% Sn (H15) heated for 120 minutes (Brazilian test). 49
Figure 59. 10% Sn (H15) heated for 30 minutes (Brazilian test). 49
Figure 60. 10% Sn (H15) heated for 120 minutes (Brazilian test). 49
Figure 61. 25% Sn (H15) heated for 30 minutes (Brazilian test). 49
Figure 62. 25% Sn (H15) heated for 120 minutes (Brazilian test). 50
Figure 63. 25% Sn (H2) heated for 30 minutes (Brazilian test). 50
Figure 64. 25% Sn (H2) heated for 120 minutes (Brazilian test). 50
Figure 65. 50% Sn (H15) heated for 5 minutes (Brazilian test). 50
Figure 66. 50% Sn (H15) heated for 30 minutes (Brazilian test). 50
Figure 67. 50% Sn (H15) heated for 120 minutes (Brazilian test). 51
Figure 68. 50% Sn (H2) heated for 30 minutes (Brazilian test). 51
Figure 69. 50% Sn (H2) heated for 120 minutes (Brazilian test). 51
Figure 70. Pure H15 heated for 30 minutes 53

Figure 71. Pure H15 heated for 120 minutes.....53
Figure 72. Pure H2 heated for 30 minutes.....54
Figure 73. Pure H2 heated for 120 minutes.....54
Figure 74. 5% Sn (H15) heated for 30 minutes.....55
Figure 75. 5% Sn (H15) heated for 120 minutes.....55
Figure 76. 5% Sn (H2) heated for 30 minutes (1).....56
Figure 77. 5% Sn (H2) heated for 120 minutes (1).....56
Figure 78. 5% Sn (H2) heated for 30 minutes (2).....57
Figure 79. 5% Sn (H2) heated for 120 minutes (2).....57
Figure 80. 7.5% Sn (H15) heated for 30 minutes.....58
Figure 81. 7.5% Sn (H15) heated for 120 minutes.....58
Figure 82. 10% Sn (H15) heated for 30 minutes.....59
Figure 83. 10% Sn (H15) heated for 120 minutes.....59
Figure 84. 25% Sn (H15) heated for 30 minutes.....60
Figure 85. 25% Sn (H15) heated for 120 minutes.....60
Figure 86. 25% Sn (H2) heated for 30 minutes.....61
Figure 87. 25% Sn (H2) heated for 120 minutes.....61
Figure 88. 50% Sn (H15) heated for 5 minutes.....62
Figure 89. 50% Sn (H15) heated for 30 minutes.....62
Figure 90. 50% Sn (H15) heated for 120 minutes.....63
Figure 91. 50% Sn (H2) heated for 30 minutes.....63
Figure 92. 50% Sn (H2) heated for 120 minutes.....64
Figure 93. Exuded tin and tin oxides (1).....64
Figure 94. Exuded tin and tin oxides (2).....65

LIST OF TABLES

Table 1. Aluminum and tin properties. Source: [5], [6].....3

Table 2. SHPB Properties. 13

Table 3. Tensile strengths for H15 samples. 30

Table 4. Tensile strengths for H2 samples. 30

Table 5. Compressive strengths of H15 samples. 31

Table 6. Compressive strengths of H2 samples. 32

Table 7. Fracture toughness parameters for 5% Sn by volume. 32

Table 8. Gas gun impact tests. 33

Table 9. Relative abundance of fragment sizes.....35

Table 10. Porosity calculations. 67

Table 11. Sample dimensions. 69

THIS PAGE INTENTIONALLY LEFT BLANK

LIST OF ACRONYMS AND ABBREVIATIONS

Al	aluminum
BSD	backscatter electron detector
C	Celsius
CIP	cold isostatic press
Cu	copper
g/cc	grams per cubic centimeter
GPa	giga Pascals
H2	spherical aluminum powder (typical diameter of ~2 microns)
H15	spherical aluminum powder (typical diameter of ~15 microns)
HE	high explosive
kN	kilo Newtons
kV	kilo Volts
Mg	magnesium
mm	millimeter
MPa	mega Pascals
NPS	Naval Postgraduate School
psi	pounds per square inch
RM	reactive material
SED	secondary electron detector
SEM	scanning electron microscope
SHPB	Split-Hopkinson pressure bar
Sn	tin
TMD	theoretical maximum density
Zr	zirconium
μm	micrometer

THIS PAGE INTENTIONALLY LEFT BLANK

ACKNOWLEDGMENTS

The author would like to thank the Office of Naval Research (N0001419WX01789, managers Chad Stoltz and Matt Beyard) and the Defense Threat Reduction Agency (HDTRA1034195, manager Jeff Davis) for their financial support of this work. Benjamin Rich is acknowledged for initial work on the aluminum/tin system during a Navy internship at NPS. The author would also like to thank Dr. Joe Hooper for his guidance and Jake Kline for his mentorship and assistance with laboratory equipment.

THIS PAGE INTENTIONALLY LEFT BLANK

I. INTRODUCTION

Conventional warhead casings have traditionally been composed of steel or tungsten for their structural strength, high density, and fragmentation properties. A recent trend in warhead development has been to examine replacement materials for steel or tungsten casings that also contribute lethality beyond the simple kinetic energy of the fragments. Warhead cases using reactive materials (RM) such as aluminum (Al) that can release large amounts of energy through metal combustion have the potential to increase lethality without adding significant mass or volume to the munition [1].

In practice, the ability to maximize energy output through efficient, rapid RM combustion remains a significant challenge. Many of the RMs currently studied are brittle metal composites, which break up into fine, combustible debris but can have limited strength and tensile ductility. This thesis examines the use of tin (Sn) as a binder for two-component RMs that use aluminum as the combustible ingredient. Tin was selected due to its low melting point, allowing it to potentially liquefy when shocked by the detonating high explosive (HE) or by impact of a fragment. This may result in dynamic creation of fracture points without relying on an intrinsically brittle material, allowing for moderate ductility in unshocked conditions.

Prior work has examined the mechanical properties of RMs made from fine, compacted Al powder [2]–[4], but little work has been published on mechanical properties of a powder metallurgy RM using tin. While combustion energy output may be improved with a shock-meltable binder, the mechanical properties prior to shock must also be considered. While certain applications (primarily enhanced air blast) call for low-strength and low-toughness RM cases, it is generally desirable to have some degree of strength and ductility in the starting material.

To assess the aforementioned metrics and to achieve an understanding of the behavior of an Al/Sn composite, several mixtures with varying tin content, heat treatments, and Al particle sizes were tested for dynamic compressive and tensile strength as well as

fracture toughness, analyzed with a scanning electron microscope (SEM), and shot in a half-inch gas gun to determine fragmentation properties.

Tin was found to be a poor binder for aluminum, generally resulting in decreased strength and increased porosity with increasing tin content. SEM imaging revealed that tin, especially in higher proportions of the Al/Sn mix, acts as a soft buffer between aluminum particles and consequently inhibits particle interlocking that contributes to strength. Despite this reduction in strength, moderate tin content in the range of 5–10% by volume with similar Al and Sn particle sizes results in a relatively homogenous product after pressing and annealing. Upon sufficient shock loading, such a configuration may lead to increased dispersion of aluminum, facilitating a desired effect of rapid combustion.

II. EXPERIMENTAL METHODOLOGY

In order to fully determine if tin could perform well as a binder for aluminum, and to provide a practical recommendation for the ideal mixture formulation and manufacturing process, several mechanical properties, physical properties, and other practical considerations needed to be tested over a wide range of experimental variables. Such variables included tin percentage (by volume) of Al/Sn mixtures, particle size of aluminum, and heat treatment. Over 100 small cylindrical samples roughly 11 mm in diameter and 5 or 10 mm in length were produced to test the various combinations of these variables in order to identify trends. For reference, Table 1 lists several physical properties for bulk aluminum and tin. Notably, tin is both softer and less stiff than aluminum, which plays a significant role in determining how a mixture of the two elements performs under both hydrostatic and dynamic stress.

Table 1. Aluminum and tin properties. Source: [5], [6].

Property	Aluminum	Tin
Bulk Density (g/cc)	2.70	7.29
Melting Point (°C)	660.4	232.0
Young's Modulus (GPa)	68	44
Mohs Hardness	2.0-2.9	1.5-1.8

A. SAMPLE PREPARATION

1. Mixture Preparation

The materials used in preparing Al/Sn mixtures for pressing are shown in Figure 1. All powder mixtures were made with gas-atomized spherical aluminum with median particle sizes of 3.5 μm (H2) or 20 μm (H15) from Valimet Inc [7]. and 99% purity tin with average particle sizes ≤ 10 μm from MilliporeSigma [8].

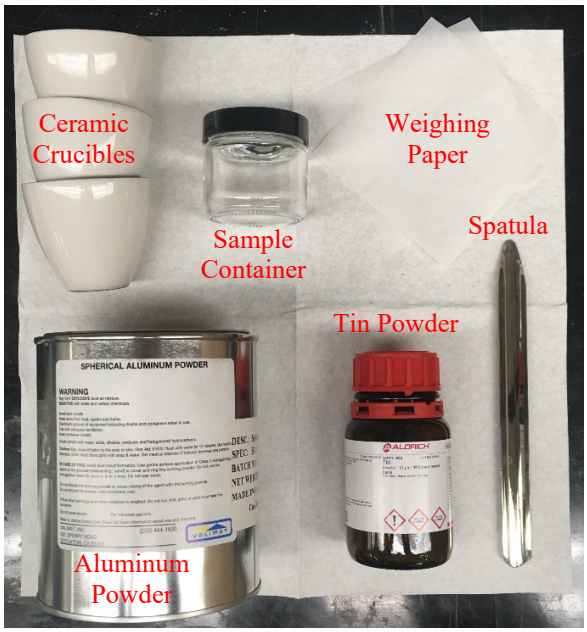

Figure 1. Mixture preparation materials.

For each desired volume percentage of tin, the Al and Sn volume fractions were converted to mass fractions so that the proper amounts of each element could be measured with a balance. Equations (1) and (2) detail the conversion from volume fractions to mass fractions, given the densities ρ_{Al}, ρ_{Sn} and volume fractions v_{Al}, v_{Sn} for aluminum and tin, respectively.

$$m_{Sn} = \frac{\rho_{Sn} v_{Sn}}{\rho_{Al} v_{Al} + \rho_{Sn} v_{Sn}} \tag{1}$$

$$m_{Al} = 1 - m_{Sn} \tag{2}$$

Once the mass fractions m_{Al} and m_{Sn} were determined, a suitable amount of either H15 or H2 aluminum powder (depending on the desired formulation) to fill a sample mold was added to a ceramic crucible using a spatula and heated for 30 minutes at 80°C in a muffle furnace to minimize water vapor in the mixture. An empty sample container was then placed on a balance and the balance was tared. The aluminum powder was then added to the sample container and the mass was recorded. The amount of tin to add to the

aluminum M_{Sn} was then determined using equation (3) given the recorded mass of aluminum M_{Al} and the mass fractions calculated previously. The actual amount of tin added was then recorded for porosity calculations.

$$M_{Sn} = M_{Al}\left(\frac{m_{Sn}}{m_{Al}}\right) \tag{3}$$

To mix the Al and Sn powders as evenly as possible, the spatula was used to carefully stir the mixture until the two powders were indistinguishable from one another, and the sample container was then closed and placed into a ball mill (shown in Figure 2) to vigorously shake the mixture for one minute.

Figure 2. Ball mill.

2. Pressing of Samples

The materials used to prepare the Al/Sn mixtures for pressing are shown in Figure 3. All Al/Sn sample mixtures were compacted into a polyurethane mold to press solid metal cylindrical rods approximately 9 cm long and 11 mm in diameter, with the exception of three point bend samples (see Chapter II.B.2) and sample warhead cases (see Chapter II.D).

Figure 3. Sample pressing materials.

Using a spatula and gloves, the Al/Sn mixture was carefully added to the mold. After each scoop of powder, the mold was gently tapped against a horizontal surface, and after every few scoops, the mold was pressed against a vibration table for several seconds to settle the powder as compactly as possible. Once the mold was filled with powder, the end cap was fitted on and pressed down, compacting the powder even more. The end cap was then removed, and more powder was added to the mold. This process was repeated as many times as necessary, using a rubber mallet to compact the end cap until it could just barely press flush against the mold. The cap-mold interface was then covered thoroughly in electrical tape (as shown in Figure 4) to ensure an air-tight seal required for pressing.

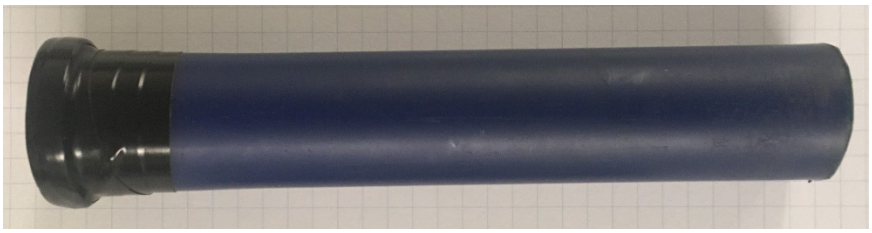

Figure 4. Sample mold prepared for pressing.

All Al/Sn samples were formed in a cold isostatic press (CIP), shown in Figure 5. A tightly sealed mold containing Al and Sn powder was placed into the liquid-filled pressure chamber and pumped to approximately 380 MPa (55,000 psi) for a duration of at least 10 minutes. The high pressure of the CIP causes the particles in the powder mixture to pack closely together and form a coherent solid.

Figure 5. Cold isostatic press (CIP).

After approximately 10 minutes, the CIP was slowly depressurized, and the mold was removed from the pressure chamber. The solidified cylindrical rod, if properly pressed, was then removed from the mold and inspected to ensure it did not have any apparent cracks or defects that would render it unusable for sample testing. Figure 6 shows an

example of a properly pressed rod. After each rod was pressed, the mold was dried of any residual fluid from the CIP and cleaned with a wire brush. This process was repeated to produce several rods of each Al/Sn mixture for creating samples.

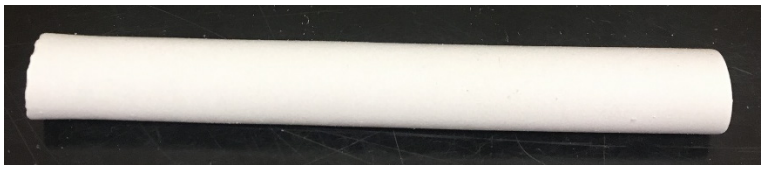

Figure 6. Pressed Al/Sn rod using CIP.

3. Machining/Cutting

A Minitom circular saw, shown in Figure 7, was used to cut each rod into several smaller samples. Pressed rods were marked at 5 mm or 10 mm intervals with a pencil and secured in place to be cut along the markings.

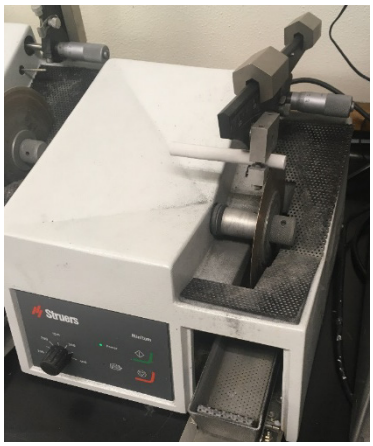

Figure 7. Cutting saw.

Each pressed rod is large enough to produce several 5 mm and 10 mm long samples, which are ideal sizes for Hopkinson Bar tests, gas gun shots, and microscopy. An example of a rod cut into several samples is shown in Figure 8.

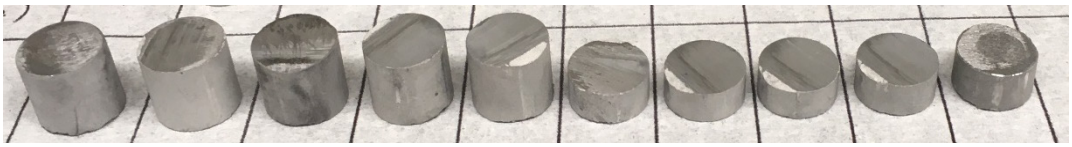

Figure 8. Samples cut from a pressed rod.

All cut samples were then polished using a rotary polisher or sandpaper to ensure flat and smooth surfaces. After polishing, the dimensions and mass of each sample were measured using a micrometer and balance, respectively, and recorded for porosity calculations. Figure 9 shows the dimensions recorded for each sample, where d_1, and d_2 are two perpendicular diameters (to determine approximate average diameter) and l is the sample length.

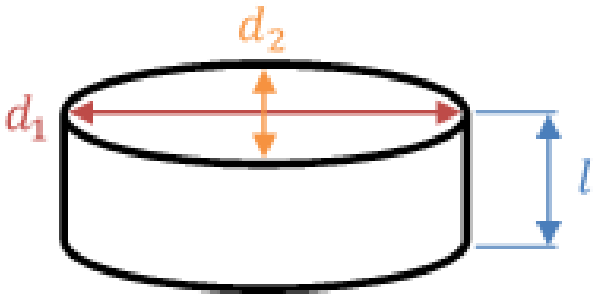

Figure 9. Sample dimensions.

4. Heat Treatment

Once cut, polished, and measured, the samples underwent various heat treatments to determine an ideal annealing process. The purpose of annealing is to reduce residual stresses caused by pressing and to promote recrystallization [9]. In efforts to avoid oxidation of the metal powders and prevent contamination, samples were initially placed in a vacuum oven (shown in Figure 10) programmed to heat for 120 minutes at 200°C under partial vacuum with argon gas.

Figure 10. Yamato vacuum drying oven.

Upon heating several samples in the vacuum oven, it was apparent that this apparatus was unsuitable for a controlled and predictable heating process. Figure 11 shows the result of a batch of samples heated in the vacuum oven, and it is visibly obvious from the colors of the samples that significant oxidation had occurred (despite meticulous efforts to prevent contamination), as well as exudation of tin onto the surface of the samples. The arrangement of samples in Figure 11 reflects the same arrangement that the samples were in inside the oven, and it is clear by the "rainbow" effect that the oven underwent uneven and uncontrolled heating, leading to a spectrum of differently oxidized samples. The exudation of tin onto the surface of the samples can be seen more clearly in Figure 12.

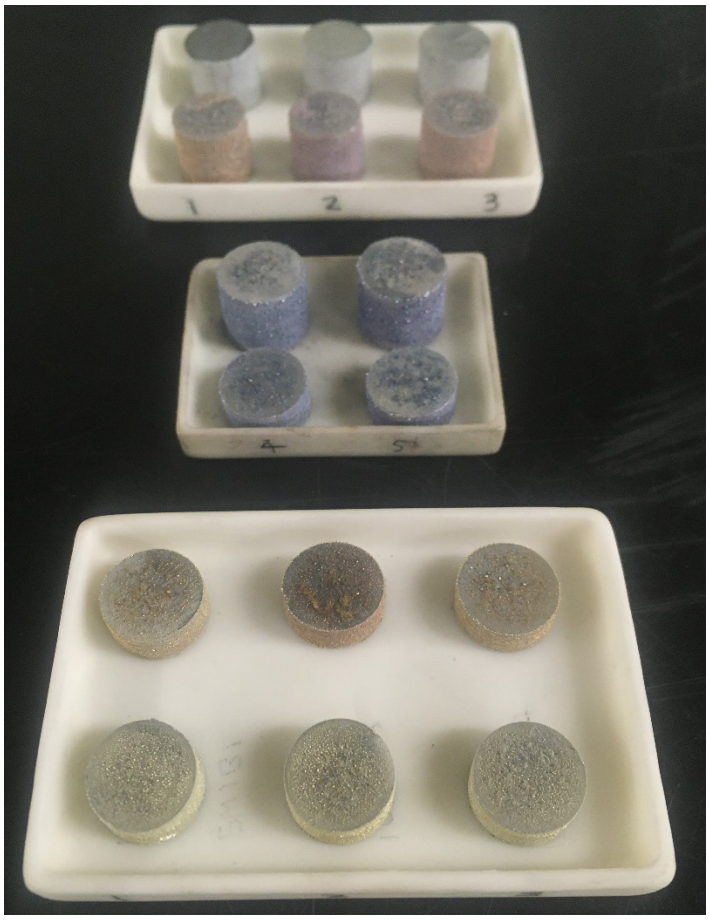

Figure 11. Exuded tin and tin oxide on surface of samples.

Figure 12. Exuded tin and tin oxide on sample surface (closeup).

To attempt a more controlled heat treatment, samples were heated in a small muffle furnace (see Figure 13) at 200°C in air for either 30 minutes or 120 minutes. Despite a far higher prevalence of oxygen in this heating method, the samples heated in the muffle furnace showed little to no oxidation or exudation of tin. This confirmed the higher reliability of the latter heating method, and all subsequent samples were heated using this method. To maximize control of heating and to prevent cross-contamination, only one or two samples were heated in the same furnace at the same time. Once heated for the desired duration, samples were immediately removed from heat and left to cool naturally at room temperature. All samples, regardless of the method of heating, were measured again (for porosity calculations) in the same manner as before heating.

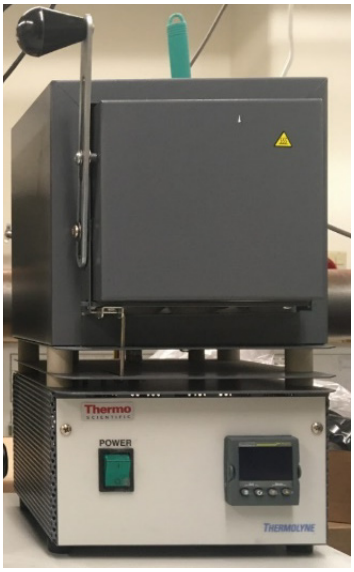

Figure 13. Small muffle furnace.

B. MECHANICAL TESTING

1. Split-Hopkinson Pressure Bar (SHPB)

To measure dynamic compressive and tensile strength for each sample, a Split-Hopkinson pressure bar (SHPB) apparatus at the Naval Postgraduate School (NPS), shown in Figure 14, was utilized with the properties listed in Table 2. It is especially important to know dynamic strengths for materials that may potentially be used in warhead casings

because these casings undergo high dynamic loads during explosive launch and high velocity impact.

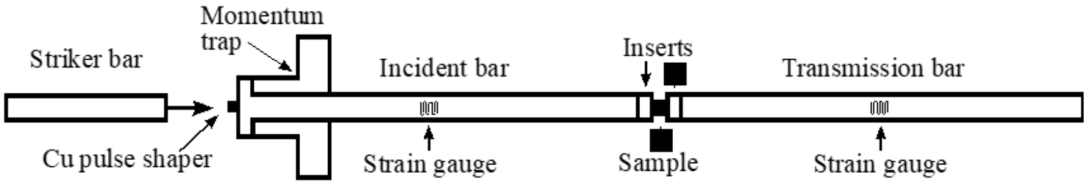

Figure 14. Split-Hopkinson pressure bar (SHPB) setup. Source: [4].

Table 2. SHPB Properties.

Property	Value
Striker Bar Density	8.278 g/cc
Striker Bar Length	304.8 mm
Striker Bar Diameter	19.05 mm
Cu Pulse Shaper Thickness	1.62 mm
Cu Pulse Shaper Diameter	17.0 mm

The striker bar was fired using a gas gun pressurized to 517 kPa (75 psi) for compression tests and 241 kPa (35 psi) for tension tests. All SHPB tests performed utilized a standard copper (Cu) pulse shaper with dimensions listed in Table 2. All tests were recorded on a Phantom v2512 ultrahigh-speed camera to ensure consistency of testing and to visualize failure mechanisms of samples.

For all compression tests, a 5 mm sample was loaded between the C350 maraging steel incident and transmission bars with a small amount of molybdenum disulfide (MoS_2) grease on each interface. The purpose of the grease is to reduce friction of metals sliding against each other under shock loading [10]. Tensile strength was estimated using a dynamic Brazilian test in which 5 mm samples were loaded axially normal to the incident

and transmission bars as shown in Figure 15. The Brazilian configuration is used to measure indirect tensile strength for brittle materials [11] and is a more suitable method for the samples tested.

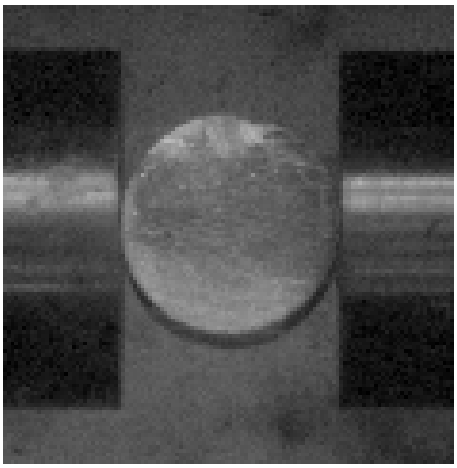

Figure 15. Brazilian tension test configuration.

2. Three Point Bend

In addition to mechanical testing of compressive and tensile strength, the fracture toughness was also tested for a pure H15 rectangular aluminum sample. The sample for this test was created by using a rectangular polyurethane mold to conform to ASTM E1820 standard dimensions [12] and pressed in a very similar process as the cylindrical rods. The exception to this standard was the notch, which was created with a circular saw as a simpler, 1 mm wide uniform cut, as shown in Figure 16.

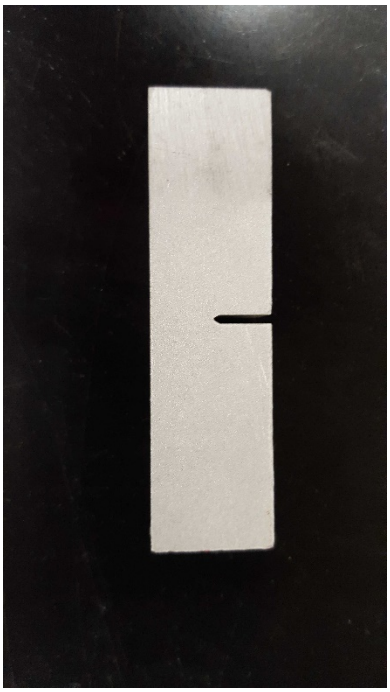

Figure 16. Three point bend H15 Al sample.

3. 0.5” Gas Gun

To examine impact and fragmentation phenomena of an Al/Sn cold-isostatically pressed sample, a 0.5” Gas Gun located at NPS (see Figure 17) was used to drive 10 mm length by 10 mm diameter samples at high velocities against a 3” thick SS 304 steel anvil and a 1/16” Al-2024 plate.

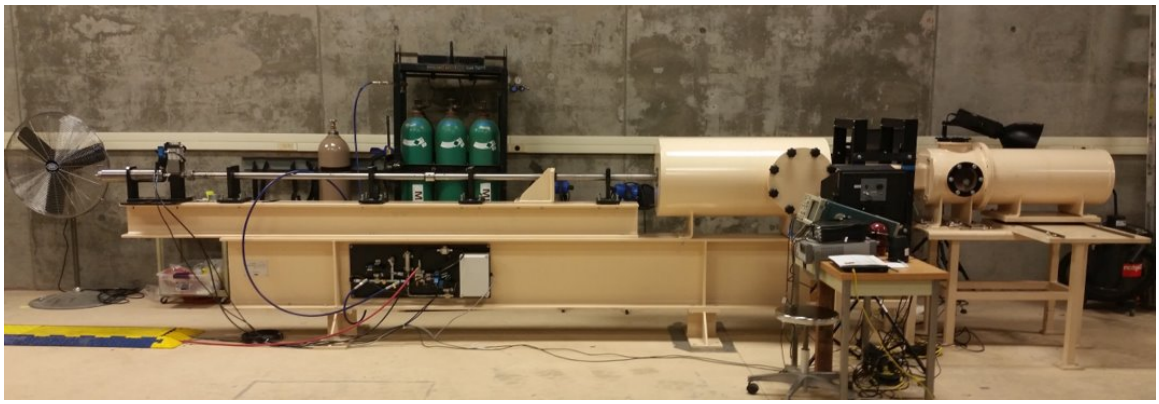

Figure 17. 0.5” Gas Gun at NPS.

Figure 18 shows a diagram of the gas gun apparatus in which the samples, shrouded in a plastic sabot, were fired via high-pressure gas, passed through a sabot stripper, and impacted onto a target at normal incidence. A light screen velocimeter measured the sample velocity prior to impact, and the impact was recorded on a Phantom v2512 camera.

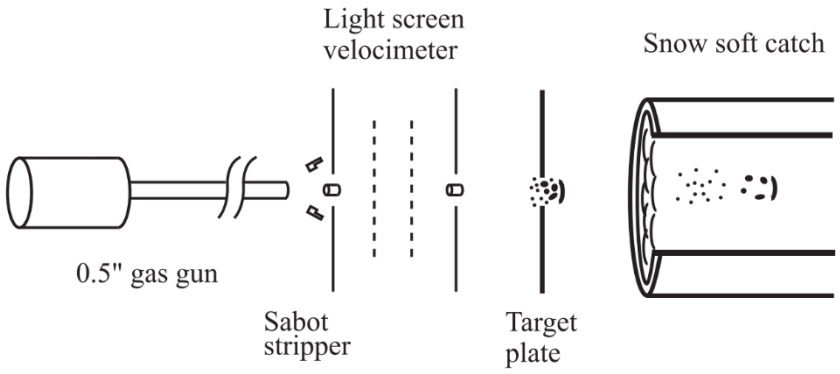

Figure 18. 0.5” Gas Gun Test Setup. Source: [13].

Samples fired against a thin aluminum plate broke apart upon impact, and the fragments were caught in a soft-catch bank of artificial snow in order to collect and analyze the fragments without post-impact deformation or contamination. The snow was evaporated away and the fragments were retrieved to be analyzed for size distribution. The collected fragments were passed through a series of stacked sieves on a vibration table (shown in Figure 19) and the mass of fragments left in each sieve (as well as the mass that passed through all sieves) was recorded.

Figure 19. Sieves and vibration table.

For samples fired against a steel anvil, no penetration occurred, and the snow catch was not utilized. As such, fragments were not retrieved for those tests.

C. SCANNING ELECTRON MICROSCOPY

To investigate how tuning different variables in the samples affect their underlying mechanisms of structural failure and to visually assess the distribution of tin within the Al/ Sn mixture, the use of a Zeiss scanning electron microscope (SEM) at NPS, shown in Figure 20, was employed with multiple detectors.

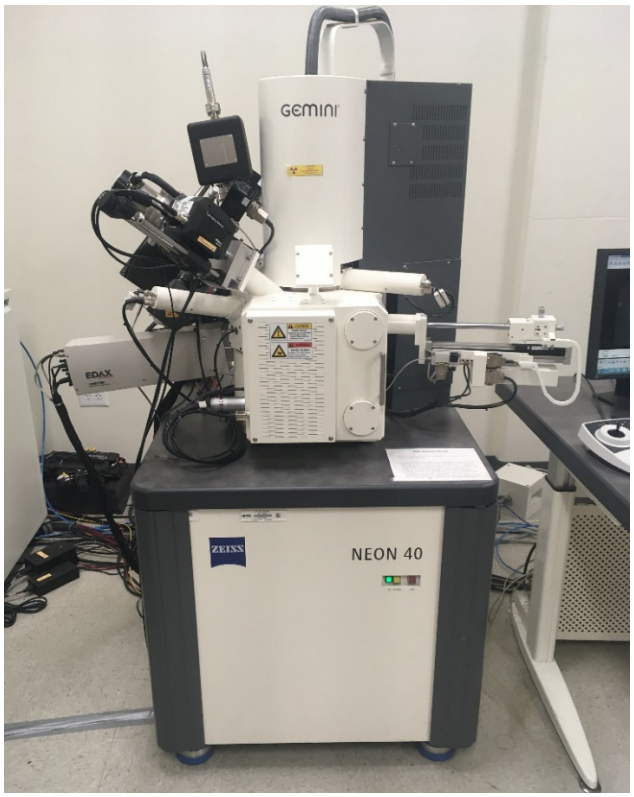

Figure 20. Zeiss scanning electron microscope (SEM).

Samples were prepared for analysis under the SEM by taking mostly fragments from Brazilian SHPB tests with flat, clean fracture surfaces, or by manually fracturing an unfractured sample if sufficiently flat crack surfaces did not exist. Fragments were then placed onto Al specimen mounts, attached via double-sided carbon tape, and placed onto a specimen holder, as shown in Figure 21.

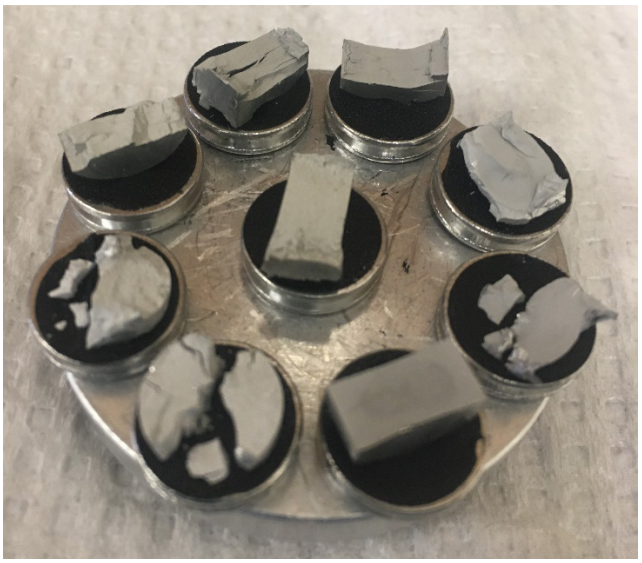

Figure 21. Mounted SEM samples.

For each sample, eight unique images were taken. For two different locations on each sample, two images (500X and 1000X magnification) each were taken with both a secondary electron detector (SED) and a backscatter electron detector (BSD). The SED allows for a clearer picture of the topography of particles and particle interfaces, whereas the BSD allows for a clearer distinction between Al and Sn to easily determine the level of distribution of Sn as well as the size of Al and Sn clusters [14]. SED images were typically taken with an accelerating voltage of 5 kV, and BSD images were usually taken with an accelerating voltage of 20 kV, both with a standard 30 μm aperture. The four images for each location on each sample (500X/1000X magnification, SED/BSD) have been stitched together for comparison and are located in Appendix B for reference.

D. SAMPLE WARHEAD CASINGS

After analysis of all sample data and images was completed, two combinations of formulation and heat treatment were selected for larger scale testing. The two combinations chosen were 5% and 10% tin by volume with H15 aluminum powder, both heated for 120 minutes at 200°C in a muffle furnace.

The powder preparation process was nearly identical to that in the sample preparation section, with modifications due to the significantly larger amount of powder required for pressing a cylindrical case vice a sample rod. Powder mixtures were measured in larger batches using a plastic measuring boat, shown in Figure 22.

Figure 22. Large batch of Al/Sn powder.

The three-part case mold (see Figure 23) was assembled by placing a steel mandrel into the center of the large hollow polyurethane cylinder, and placing the cap snugly onto the end of the hollow cylinder after the powder mixture was carefully compacted inside, using methods similar to those used for pressing the cylindrical samples. The mold assembly was then sealed with electrical tape, as shown in Figure 24, and pressed in the CIP as before.

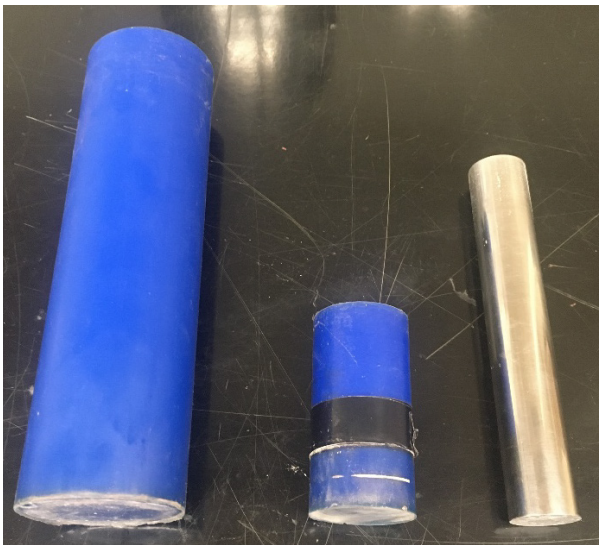

Figure 23. Mold for pressing warhead case.

Figure 24. Warhead case mold prepared for pressing.

Pressing the cases proved to be significantly more challenging than pressing the sample rods, and many attempts to press a coherent case resulted in failures such as the one shown in Figure 25. This is likely due to (1) the larger amount of powder used, allowing more opportunities for defects and (2) the shape of the case, which is hollow and thinner

than the sample rods, resulting in a higher vulnerability to large stresses during the pressurization and depressurization in the CIP.

Figure 25. Warhead case fractured during pressing.

Figure 26 shows a coherent, successfully pressed case without cracks or defects. These cases will be filled with high explosives and tested for fragmentation and failure mechanisms.

Figure 26. Pressed warhead case.

III. RESULTS AND DISCUSSION

A. POROSITY

An important metric in determining the quality of samples and how they are affected by tin content, particle size, and heat treatment is porosity. Porosity is the ratio of the volume of voids in a porous body to the total volume of the body [15]. To calculate porosity, the theoretical maximum density (TMD) was first calculated using equation (4) with the densities and actual volume fractions of tin and aluminum for each set of samples made from the same Al/Sn mixture.

$$\rho_{TMD} = v_{Al}\rho_{Al} + v_{Sn}\rho_{Sn} \tag{4}$$

The measured density ρ_m for each sample can be calculated using equation (5), where m is the measured mass of the sample and l, d_1, and d_2 are the measured dimensions of the sample, according to Figure 9 (in Chapter II.A.3). This density is then used to calculate the porosity for each sample using equation (6).

$$\rho_m = \frac{4m}{\pi(d_1 + d_2)^2 l} \tag{5}$$

$$Porosity = \left(1 - \frac{\rho_m}{\rho_{TMD}}\right) \times 100\% \tag{6}$$

The porosity was calculated for each sample before and after heating, and several comparisons were made between heat treatments, tin content, and aluminum particle size (H15 versus H2). Figure 27 shows the porosity of every sample before and after heating as a function of tin content. It is not immediately apparent what trends can be drawn from this raw porosity data, other than a seemingly higher porosity in general after heating than before heating for a given tin percentage, and a slight increase in porosity with higher tin content.

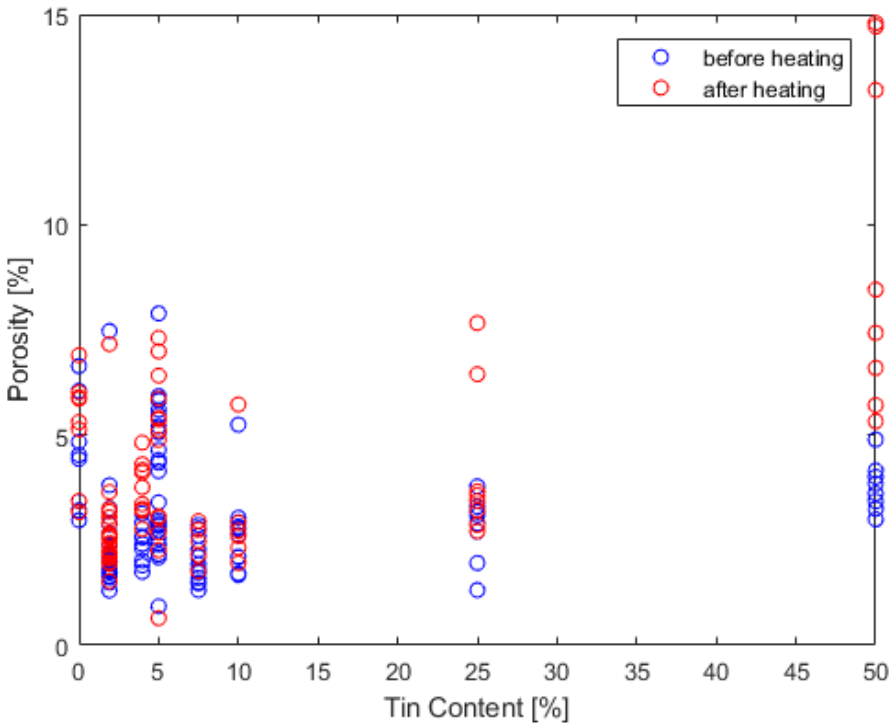

Figure 27. Porosity before and after heating (all samples).

However, when examining the *change* in porosity for a given tin percentage after heating, there is a much clearer trend. Figure 28 shows the percent change in porosity as a function of tin content, with standard error bars for all samples of each tin content. It is clear from Figure 28 that in general, as tin content increases, the change in porosity from before heating to after heating increases significantly for all samples.

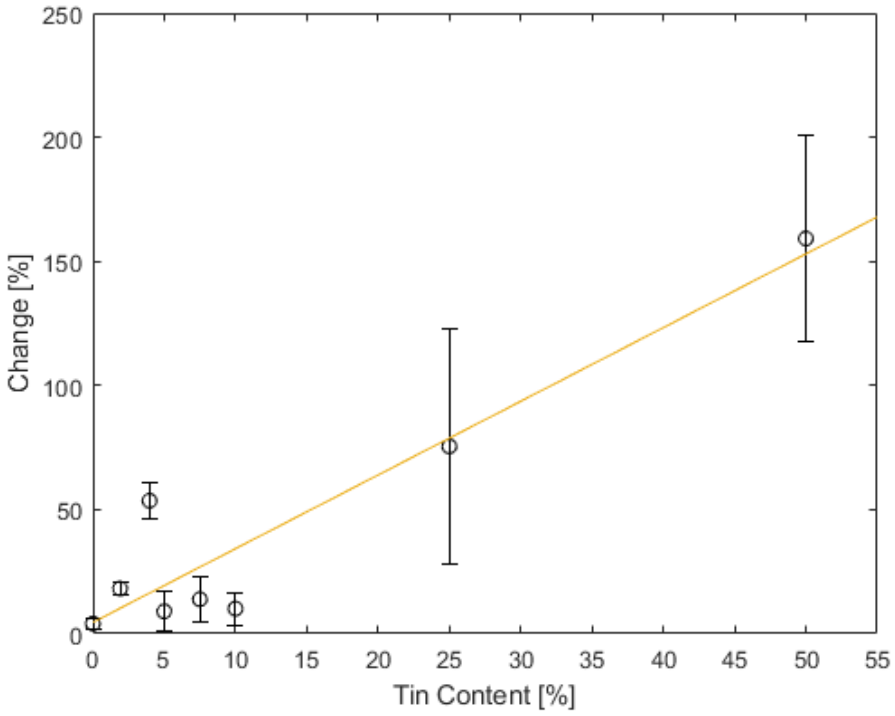

Figure 28. Change in porosity after heating.

Investigating further, the effect of aluminum particle size as well as heating duration can be seen in Figures 29–32. Figures 29 and 30 show the change in porosity after heating as a function of tin content for H2 samples heated for 30 minutes and 120 minutes in a muffle furnace, respectively. The porosity remains relatively constant after heating with lower tin percentages but increases more drastically with higher tin percentages. The variation in porosity change also appears to be higher at the highest tin content (50% by volume).

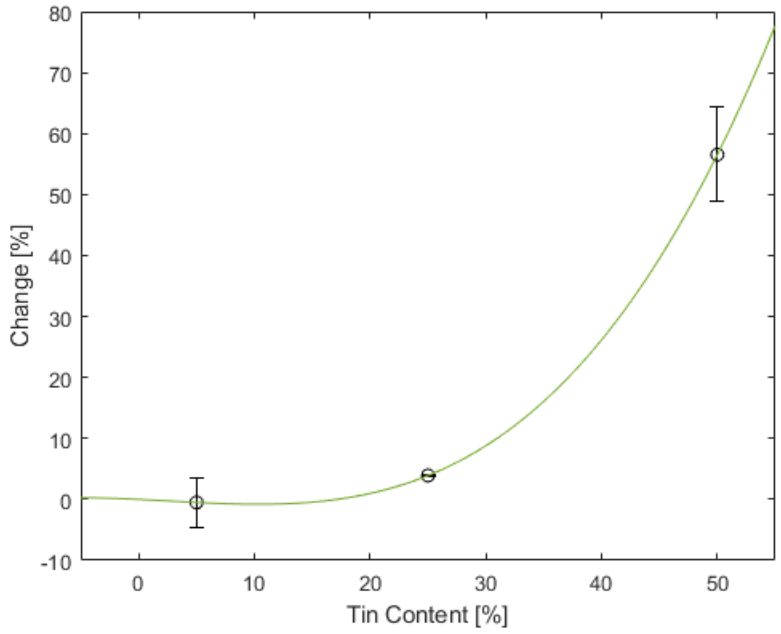

Figure 29. Change in porosity after heating for 30 minutes at 200°C (H2 samples).

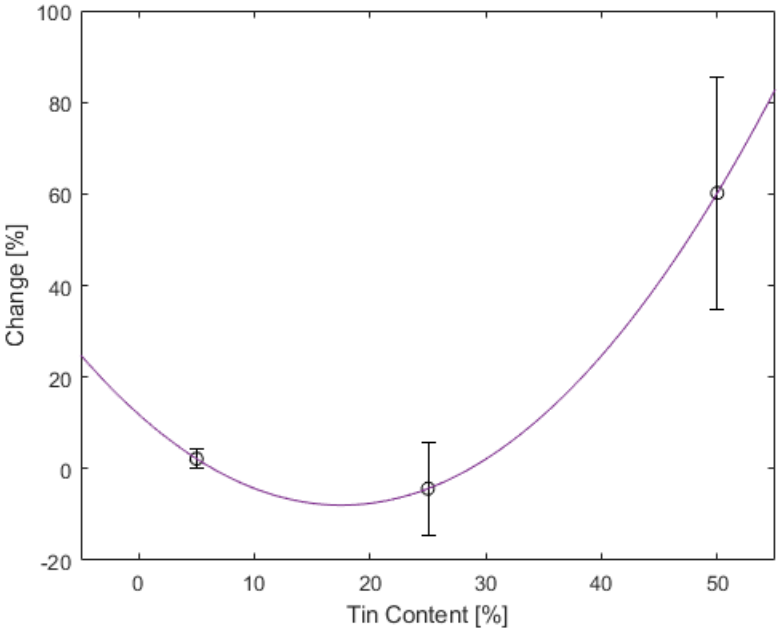

Figure 30. Change in porosity after heating for 120 minutes at 200°C (H2 samples).

Likewise, Figures 31 and 32 show this relationship for H15 samples heated for 30 minutes and 120 minutes, respectively. The trends are similar yet even more defined, in that porosity change after heating increases with higher tin content.

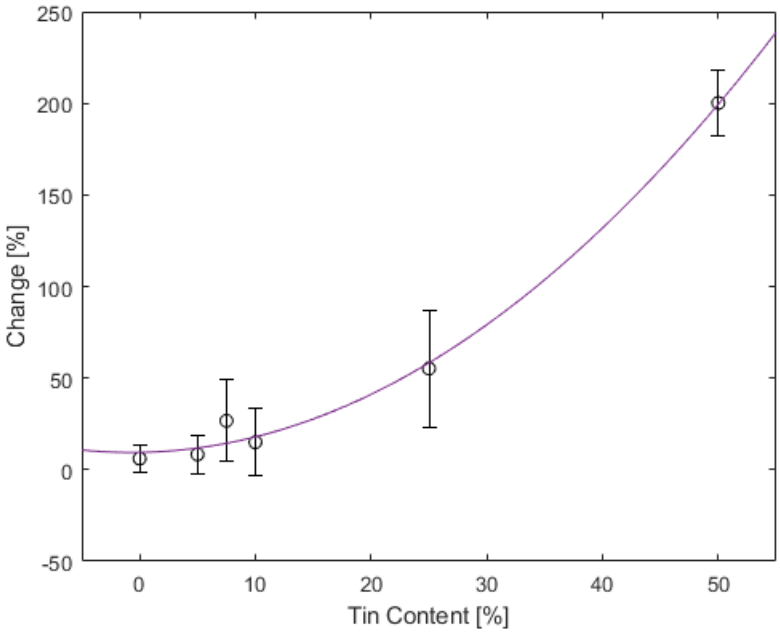

Figure 31. Change in porosity after heating for 30 minutes at 200°C (H15 samples).

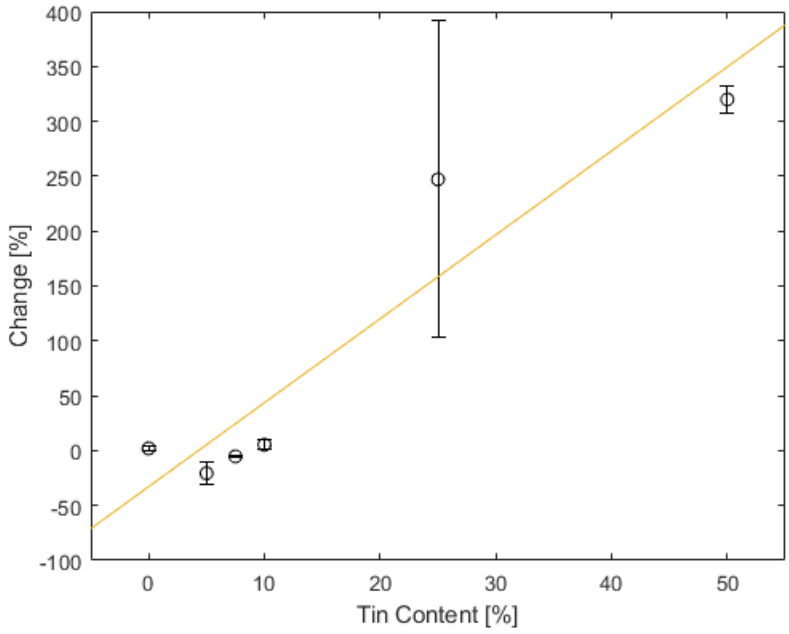

Figure 32. Change in porosity after heating for 120 minutes at 200°C (H15 samples).

The agreement of trends for both H15 and H2 samples in that porosity change increases with tin content suggests that the main contributor to this effect is tin, and not aluminum. For nearly all samples the change in mass after heating was negligible, meaning that the porosity change was mainly a function of volumetric expansion. This suggests that, upon heating, either the tin permanently expands, or the tin-aluminum particle interfaces cause an increase in overall volume. This phenomenon is investigated further with scanning electron microscopy in Chapter II.C.

B. MECHANICAL PROPERTIES

1. Tensile Strength

Tensile strength was estimated for all samples heated in a muffle furnace using equation (7) from the ASTM D3967 standard Brazilian test method [16], where P_{max} is the peak force experienced by the sample before failure, d is the diameter of the sample (taken as the arithmetic mean of two perpendicular measured diameters), and b is the thickness of the sample.

$$\sigma_T = \frac{2P_{\max}}{\pi db} \tag{7}$$

Figure 33 shows the calculated tensile strengths of all samples heated in the muffle furnace for 30 or 120 minutes that failed under a Brazilian test. It is clear from the data that for samples with both H2 and H15 Al, regardless of heating duration, there is a general trend of decreasing tensile strength with increasing tin content. It is also clear that for a given tin percentage, samples with H2 Al have a higher tensile strength than samples with H15.

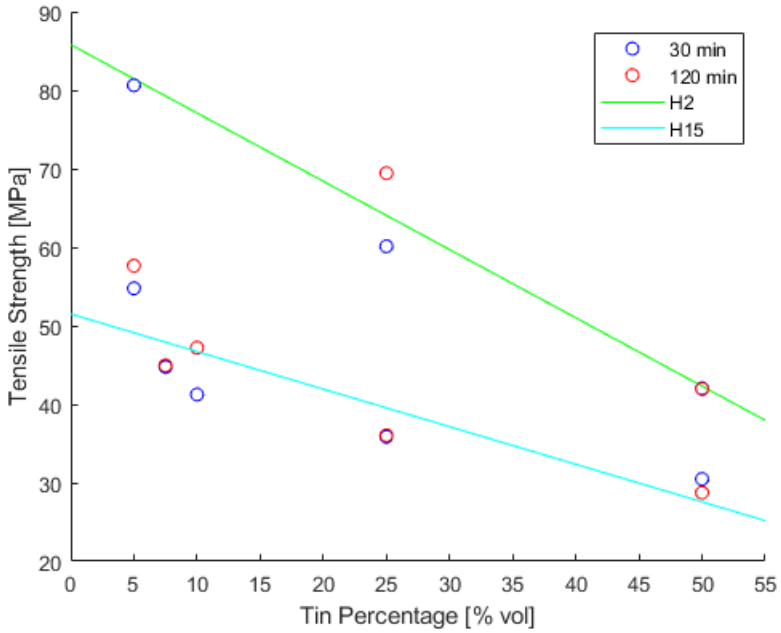

Figure 33. Tensile strengths.

Table 3 lists the calculated tensile strengths σ_T for H15 samples, and Table 4 lists the calculated tensile strengths for H2 samples, both with 30 and 120 minute heating durations. Samples that did not fail under a Brazilian test are denoted with an asterisk and would likely have a higher strength before failure.

Table 3. Tensile strengths for H15 samples.

Sn Content	σ_T [MPa] (30 min)	σ_T [MPa] (120 min)
0%	67.52*	59.79*
5%	54.76	57.64
7.5%	44.74	44.95
10%	41.24	47.20
25%	35.87	36.05
50%	30.49	28.73

* Sample did not fail

Table 4. Tensile strengths for H2 samples.

Sn Content	σ_T [MPa] (30 min)	σ_T [MPa] (120 min)
0%	73.69*	74.70*
5% (1)	79.08*	76.10*
5% (2)	80.63	75.78*
25%	60.12	69.43
50%	42.02	41.94

* Sample did not fail

2. Compressive Strength

Samples generally did not fail under compression tests, and as a result, compressive strengths were taken as the true stress at 5% true strain for consistency. Figure 34 shows these compressive strengths for all samples heated in the muffle furnace for 30 or 120 minutes. The trends for compressive strength follow those observed for tensile strength: strength generally decreases with increasing tin content, regardless of heating duration, and H2 samples have a higher strength than H15 samples for a given tin percentage.

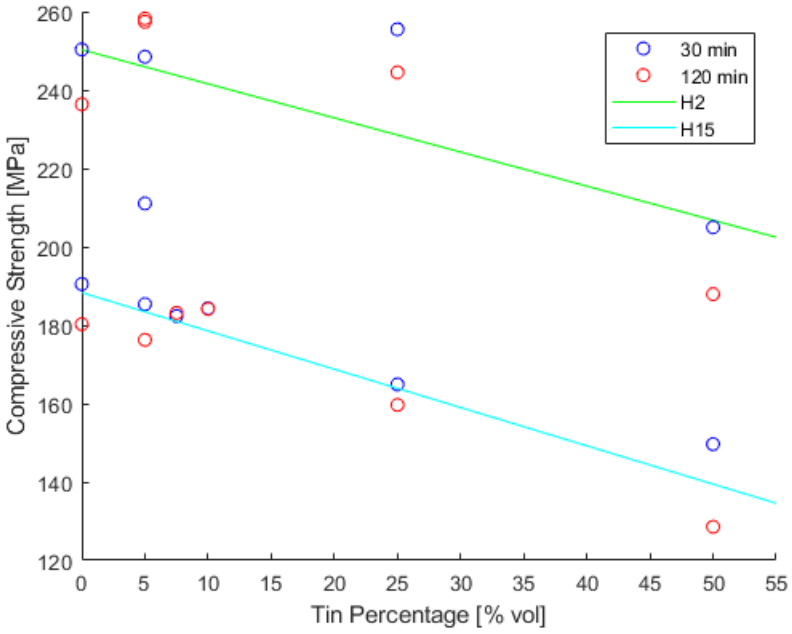

Figure 34. Compressive strengths.

Table 5 lists the compressive strengths σ_C for H15 samples, and Table 6 lists the compressive strengths for H2 samples, both with 30 and 120 minute heating durations.

Table 5. Compressive strengths of H15 samples.

Sn Content	σ_C [MPa] (30 min)	σ_C [MPa] (120 min)
0%	190.49	180.26
5%	185.36	176.26
7.5%	182.33	183.11
10%	184.32	184.16
25%	164.90	159.65
50%	149.65	128.56

Table 6. Compressive strengths of H2 samples.

Sn Content	σ_C [MPa] (30 min)	σ_C [MPa] (120 min)
0%	250.33	236.36
5% (1)	211.06	257.41
5% (2)	248.47	258.21
25%	255.48	244.49
50%	204.98	187.93

3. Fracture Toughness

Fracture toughness was calculated for two 5% Sn by volume rectangular samples by performing a three point bend test in accordance with ASTM E1820 standards [12], with the exception of the notch, as noted in Chapter II.B.2. Fracture toughness was calculated using equation (8):

$$K_{(i)} = \left[\frac{P_i S}{(BB_N)^{1/2} W^{3/2}} \right] f(a_i / W) \tag{8}$$

where

$$f\left(\frac{a_i}{W}\right) = \frac{3(a_i/W)^{1/2}\left[1.99 - (a_i/W)(1-a_i/W)(2.15 - 3.93(a_i/W) + 2.7(a_i/W)^2)\right]}{2(1+2a_i/W)(1-a_i/W)^{3/2}} \tag{9}$$

Table 7 lists the parameters used in equations (8) and (9) to calculate the fracture toughness.

Table 7. Fracture toughness parameters for 5% Sn by volume.

Parameter	Sample 1	Sample 2
Maximum force, P_i [kN]	0.546	0.607
Grip separation, S [cm]	5.080	5.080
Block width, $B = B_N$ [cm]	1.064	1.046
Block height, W [cm]	1.889	2.143
Crack length, a_i [cm]	0.881	1.124
Fracture Toughness, K [MPa·m$^{1/2}$]	**2.410**	**2.709**

4. Gas Gun and Fragmentation Analysis

A total of three gas gun tests were performed for 10% tin by mass (approximately 3.9% by volume) with H15 aluminum to determine impact and fragmentation properties. Table 8 lists the impact velocities, V_0, and post-perforation residual velocities, V_r (if applicable), as well as the target that the sample was impacted upon. All samples were shot against a target at normal incidence.

Table 8. Gas gun impact tests.

Shot	V_0 (m/s)	V_r (m/s)	Target Info
1	-	-	3” Thickness SS 304 Anvil
2	548	-	3” Thickness SS 304 Anvil
3	713	550	1/16” Al-2024 plate

The first shot against a steel anvil failed due to a misalignment of the sabot stripper, causing premature impact and fragmentation of the sample, as can be seen in Figure 35.

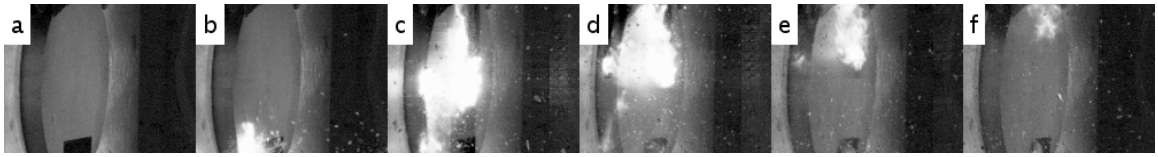

Figure 35. Gas gun shot 1.

With the sabot stripper realigned, the same test was performed (shown in Figure 36) in which the sample fragmented upon impact against the steel anvil.

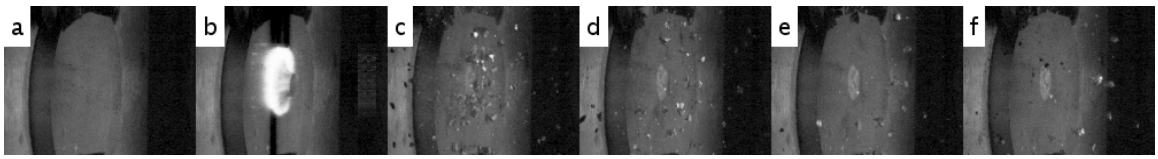

Figure 36. Gas gun shot 2.

The third shot was against a thin aluminum plate and achieved complete perforation, as shown in Figure 37.

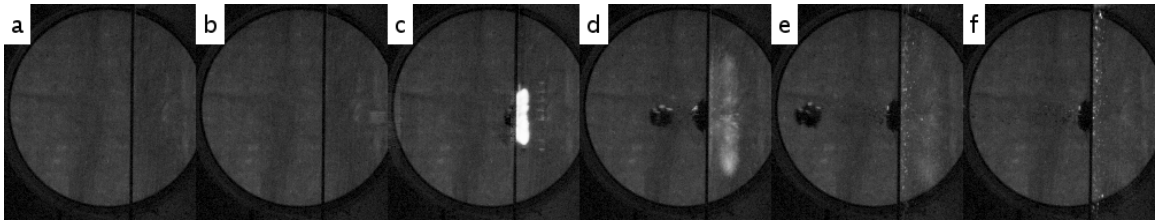

Figure 37. Gas gun shot 3.

Fragments collected via soft snow-catch from the third gas gun shot (shown in Figure 38) were analyzed for mass distribution using a series of sieves and a vibration table. From the initial mass of the 10 mm long by 10 mm in diameter sample of approximately 2.8 g, the total collected fragment mass was 2.1 g (about 75%).

Figure 38. Fragments collected from gas gun impact.

Figure 39 shows the mass distribution of fragments caught in each sieve, and Table 9 lists the percentage of the total collected mass left in each sieve. Approximately 50% of the total collected mass corresponds to particle sizes between 300 and 425 microns.

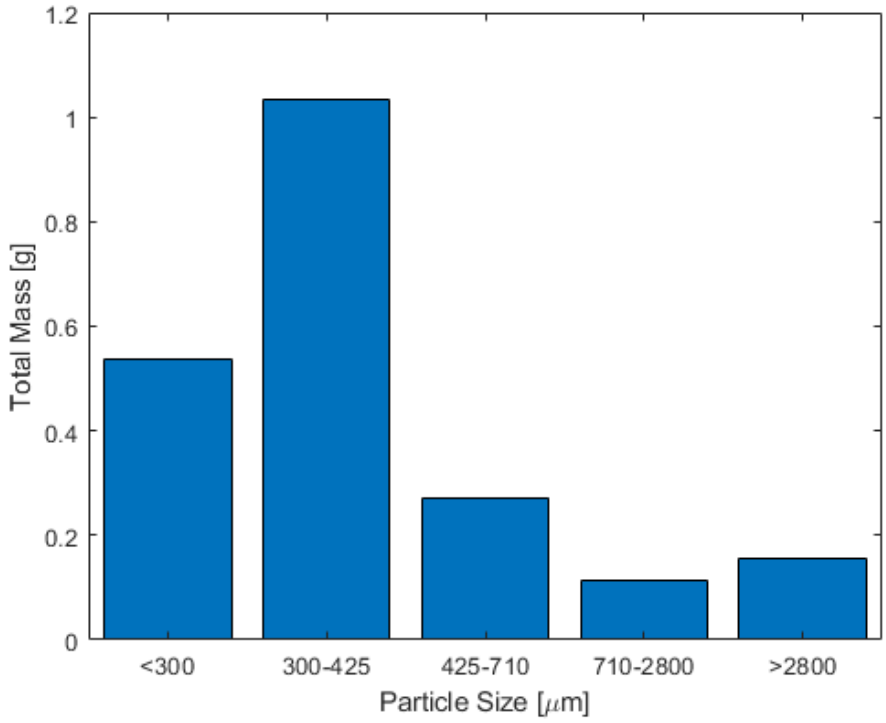

Figure 39. Gas gun impact fragment distribution.

Table 9. Relative abundance of fragment sizes.

Size [μm]	Mass [g]	% Total Mass
300-425	1.0339	49.99%
< 300	0.5360	25.40%
425-710	0.2719	12.88%
> 2800	0.1544	7.32%
710-2800	0.1143	5.42%

C. SEM IMAGING

After comparing SEM images for all samples, several trends were identified that help explain the trends in mechanical properties and provide new insights into considerations for future applications.

Figure 40 shows a progression of tin content from top to bottom of H15 Al with 0%, 5%, 7.5%, 10%, 25%, and 50% Sn by volume, all heated for 30 minutes at 200°C. The left column (a, c, e, g, i, k) includes images taken using the SED, and the right column (b, d, f, h, j, l) includes images taken using the BSD. It is clear from this progression that the H15 Al particles are very angular in shape with 0% Sn and become more spherical with increasing tin content. This essentially shows that tin acts as a soft cushion between Al particles. Pure H15 has no cushioning, resulting in direct contact and thus high deformation between Al particles during cold isostatic pressing, whereas high tin content (50% by volume) provides enough cushioning to prevent direct contact between Al particles and preserve their spherical shape during pressing. It is also apparent that the more angular particles in lower tin content samples exhibit significantly higher interlocking between Al particles than that of higher tin content samples. This increased interlocking at lower tin percentages helps to explain the trends of compressive and tensile strengths from the SHPB tests as more interlocking (as a result of angular particle surfaces) predicts higher strength [17].

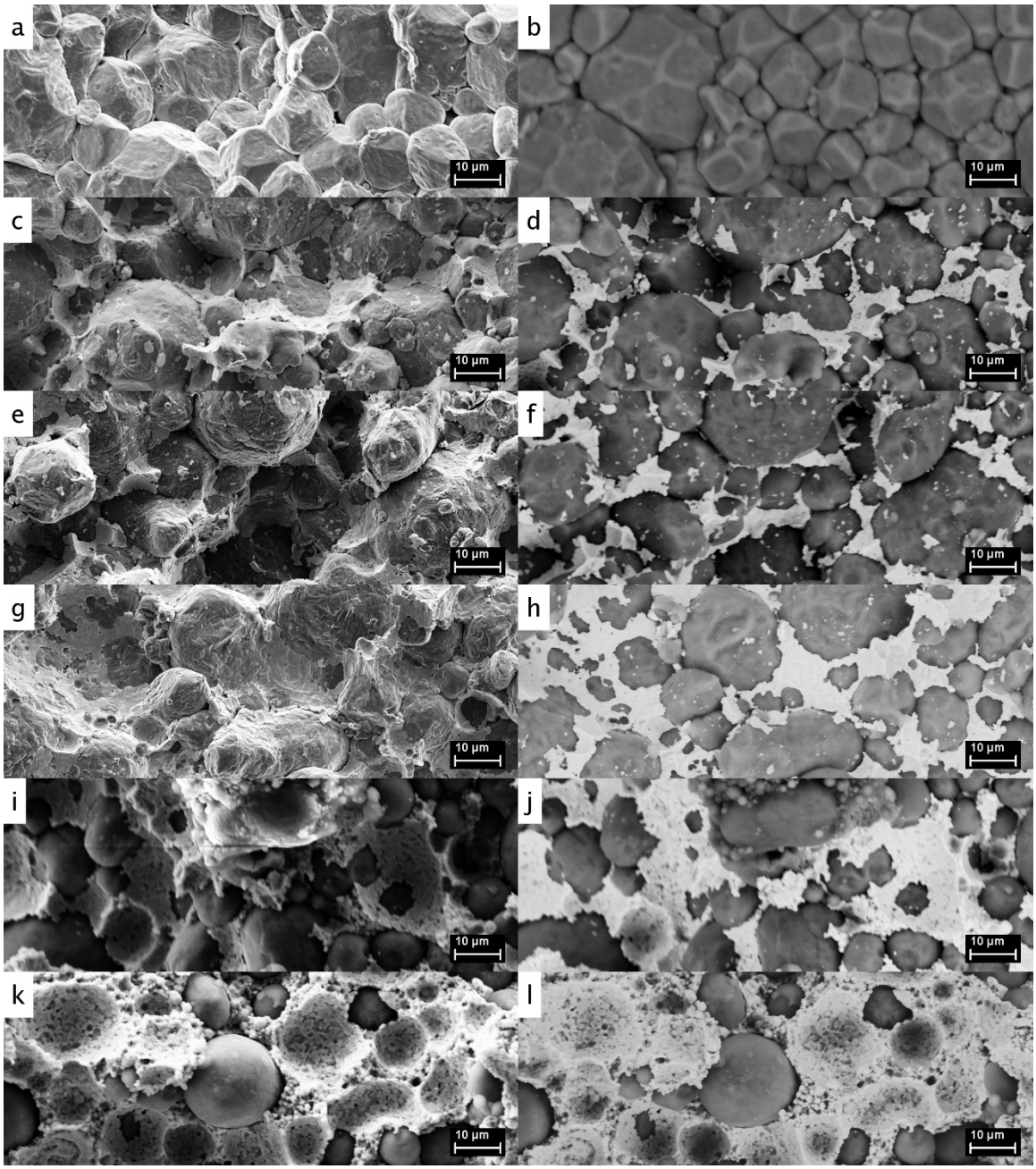

Figure 40. Progression of tin content for H15 samples heated for 30 minutes.

This trend is also equally as apparent with H15 samples heated for 120 minutes, shown in Figure 41, which corroborates the similarity in strengths between 30 minute and 120 minute heating durations and a similar trend of decreasing strength (compressive and tensile) with increasing tin content.

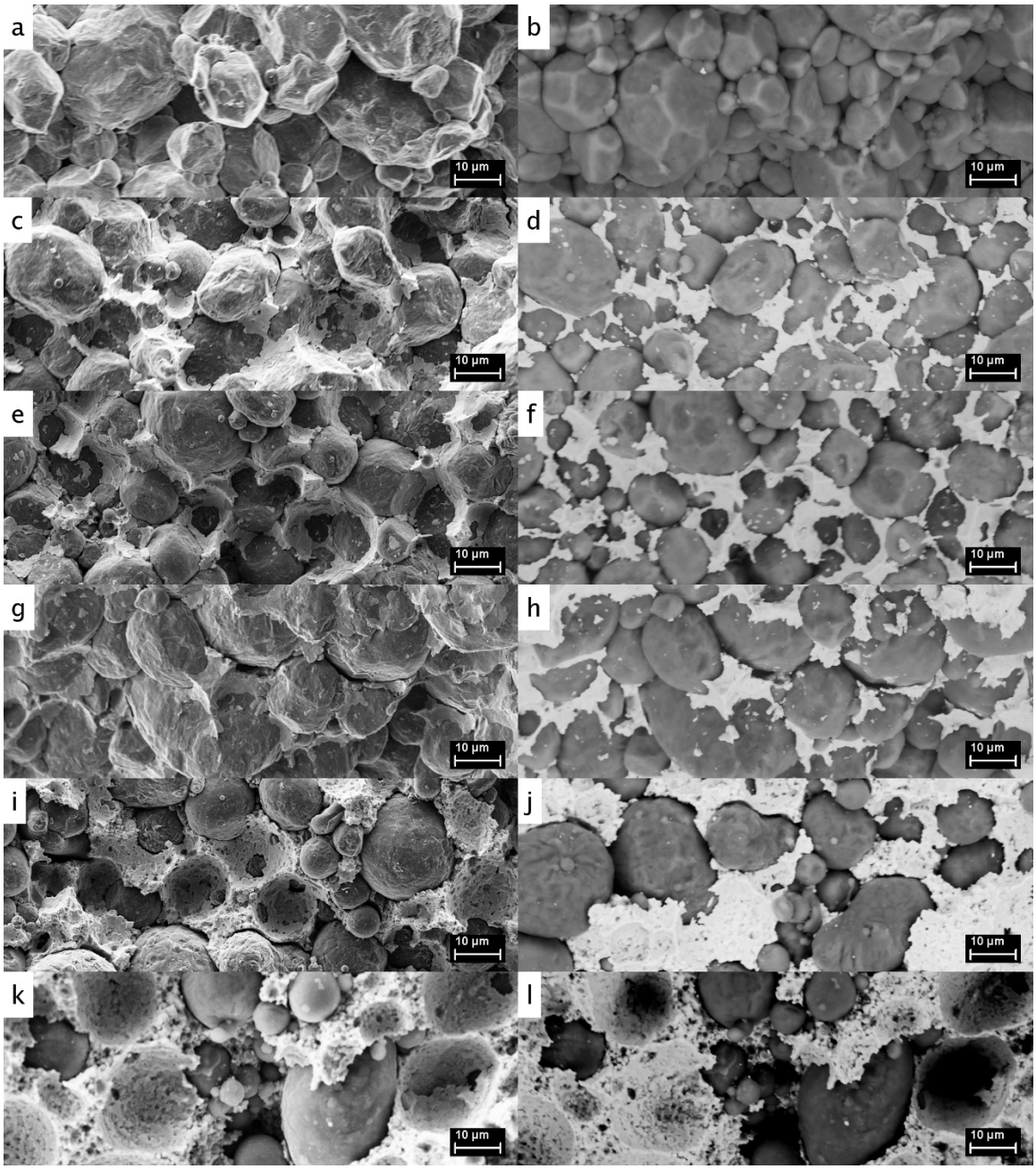

Figure 41. Progression of tin content for H15 samples heated for 120 minutes.

Figure 42 shows a similar progression of increasing tin content (0%, 5%, 25%, and 50% by volume) with H2 Al and heated for 30 minutes from top to bottom, with the images in the left column (a, c, e, g) taken using the SED and those in the right column (b, d, f, h) taken using the BSD. The trend observed with H15 samples is not as obviously apparent with H2 samples (likely due to their small size), but still recognizable, in that pure H2 (a,

b) appears to have more angular shaped particles than higher tin percentages, and the Al particles appear to become more spherical and smooth with higher tin percentages. Although, even with higher tin content, there are still frequent clusters of Al particles in direct contact with each other due to the small size of H2 particles relative to the pre-pressed tin particles. It is also likely that there is more interlocking among H2 Al particles than H15 particles as more surface area per unit volume of Al is exposed. This increased interlocking, even at high tin content, helps explain why the strengths of H2 samples were consistently higher than those of H15. H2 samples heated for 120 minutes (shown in Figure 43) look very similar and follow similar patterns as those heated for 30 minutes, and thus the same inferences apply, which makes sense as the samples heated for 30 minutes and 120 minutes seem to follow the same trendline.

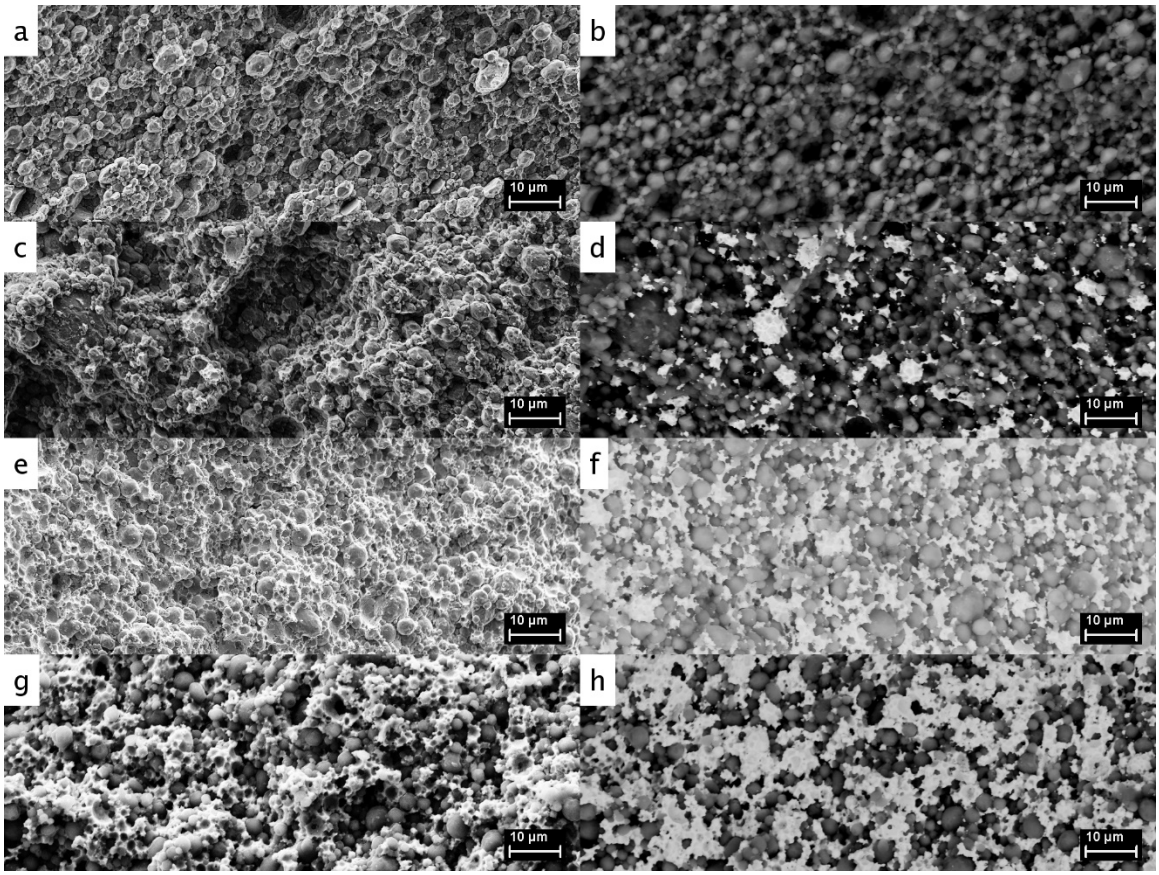

Figure 42. Progression of tin content for H2 samples heated for 30 minutes.

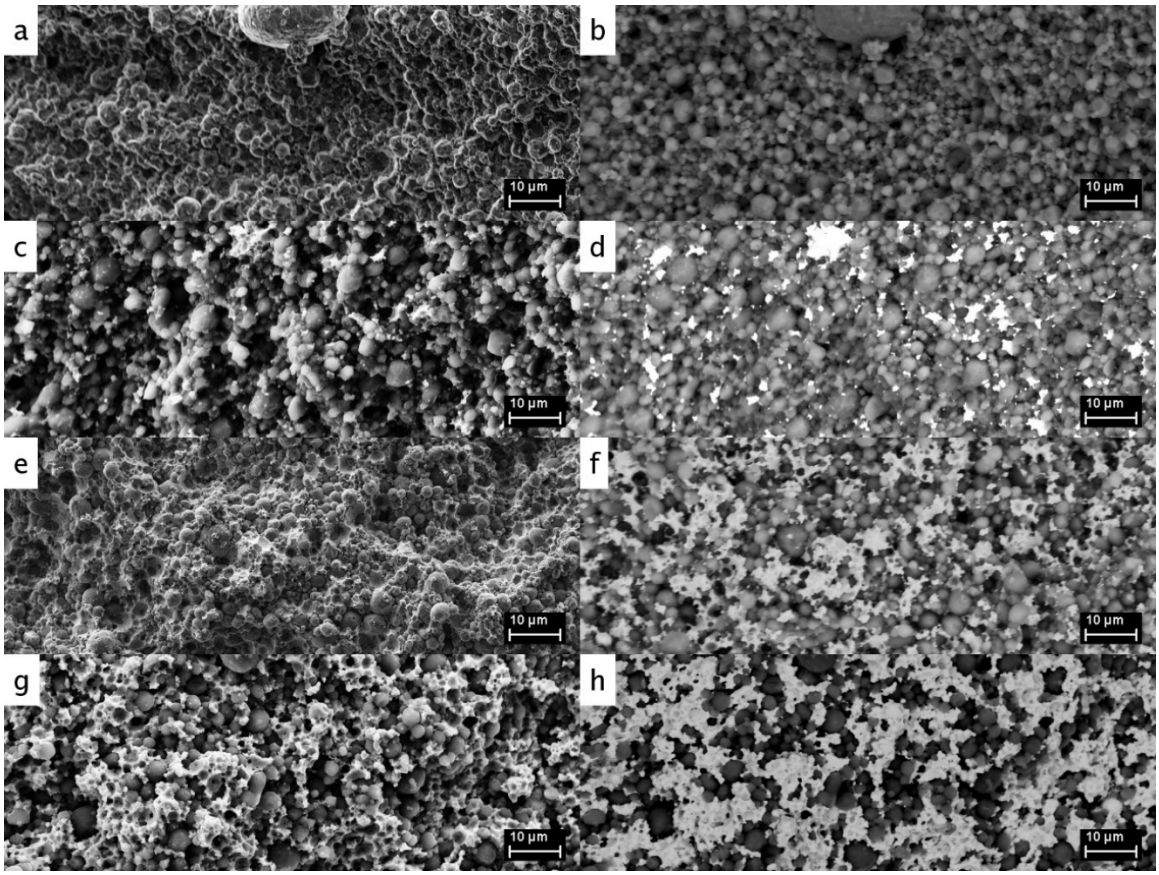

Figure 43. Progression of tin content for H2 samples heated for 120 minutes.

One particularly noticeable difference between H15 samples and H2 samples was the degree of distribution of tin. Figure 44 shows a comparison between H15 samples (left column) and H2 samples (right column) with 5% Sn (top row) and 25% Sn (bottom row). It is clear that the tin (lighter color) is very well distributed between the aluminum (darker color) for the 5% Sn with H15 sample compared to the 5% Sn with H2 sample, where separate clusters of Sn and Al are frequent. For the 25% Sn with H15 sample, the tin is still relatively well distributed, and the 25% Sn with H2 sample is more equally distributed, although there are still separate clusters of Al and Sn.

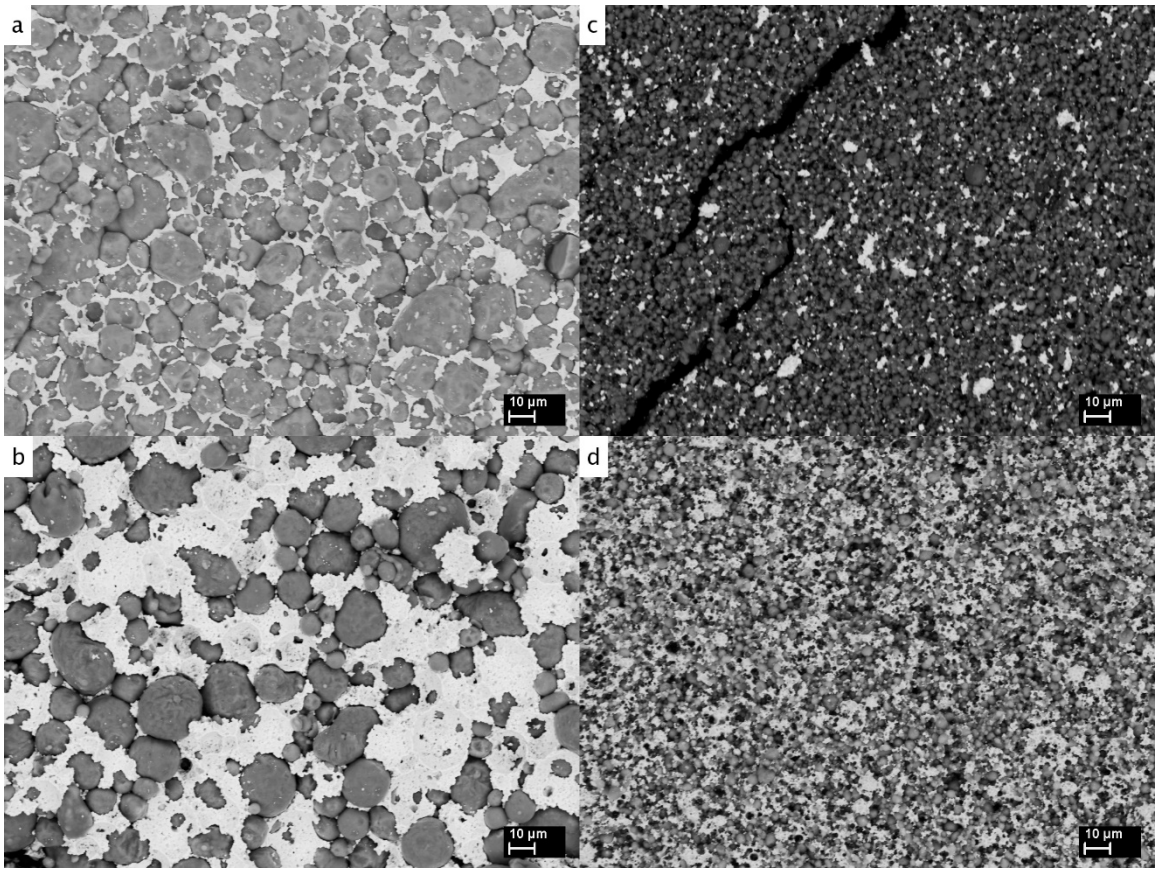

Figure 44. Distribution of tin in H15 (a, b) and H2 (c, d) with 5% (a, c) and 25% (b, d) Sn heated for 120 minutes.

This difference in distribution of tin is apparent for 30 minute heating and for other tin percentages as well and shows that the H15 samples are generally more homogenous than the H2 samples. The lower homogeneity of H2 samples may help explain a higher variance from the trendline for compressive and tensile strengths.

Particles from the brightly colored surface of a sample heated in the vacuum oven were also analyzed to confirm their structure. Figure 45 shows an SED image of these particles, the more spherical of which are presumed to be exuded tin, and the longer and thinner of which are presumed to be tin oxides.

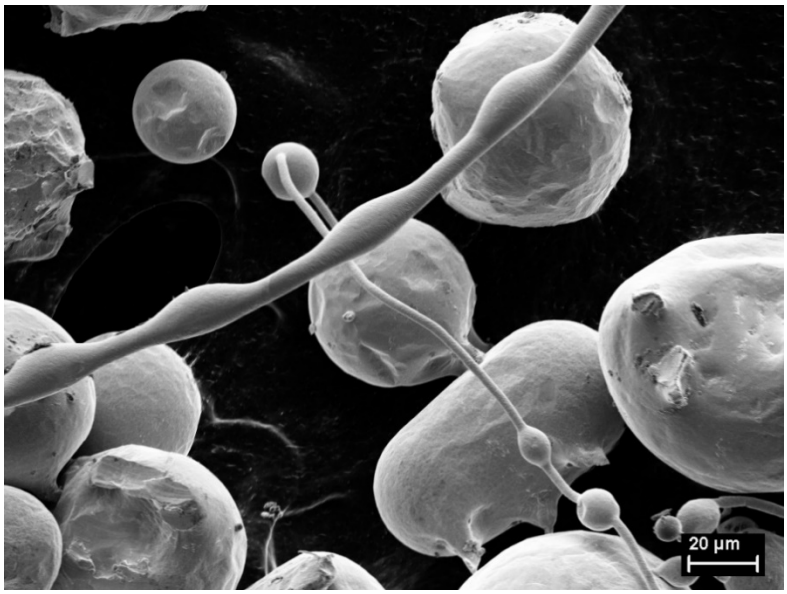

Figure 45. Exuded tin and tin oxide (SED).

The porosity data showed that both porosity after heating and change in porosity increase significantly with increasing tin content, particularly with H15 samples. To investigate this phenomenon, a 50% Sn with H15 sample was heated for only five minutes for 200°C in a muffle furnace to compare with samples of the same tin content and Al particle size heated for 30 and 120 minutes. A sample with 50% Sn and H15 was chosen for the comparison because the largest porosity and change in porosity were found in this formulation, and it is assumed that any physical explanation for these trends would be most obvious with such parameters. Figure 46 shows a comparison between 5-, 30- and 120-minute heating durations with 50% Sn and H15 Al. From this comparison it appears that there are very slightly larger gaps in the interface between Al (darker color) and Sn (lighter color) in the samples that underwent a longer heating duration than that which underwent only five minutes of heating. These gaps may be explained by the impressions in the tin where spherical aluminum particles once were, which are much smoother in (a) than (b) and (c). The rougher surface of the impressions (and by extension, Al/Sn interfaces) in samples heated for longer durations would result in less overall contact with Al particles and thus more empty space along each interface, explaining a higher porosity.

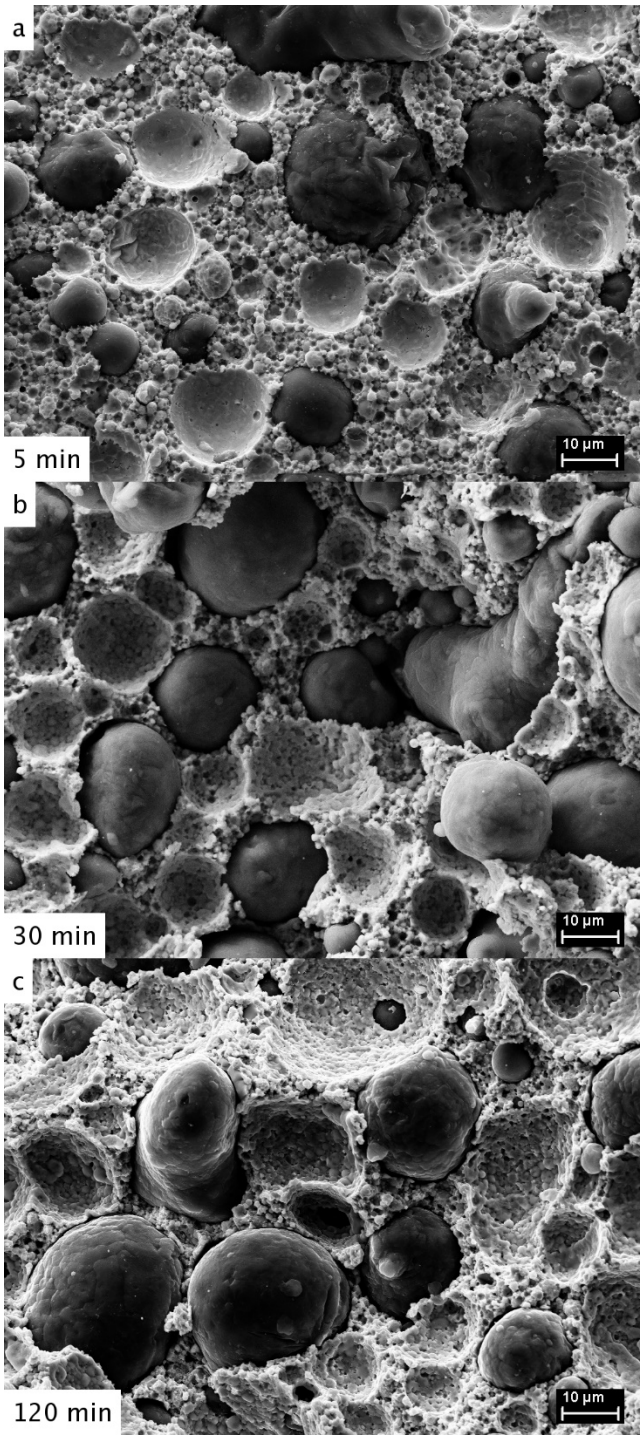

Figure 46. 50% Sn (H15 Al) heated for 5, 30, and 120 minutes.

THIS PAGE INTENTIONALLY LEFT BLANK

IV. CONCLUSIONS AND FUTURE WORK

Porosity was generally found to increase after heating, although the duration of heating did not have a substantial effect on mechanical strength. The use of H2 aluminum powder clearly results in a higher compressive and tensile strength than H15 powder for a given tin percentage; however, tin was found to be much more homogenously distributed among H15 than among H2. Thus, H2 is presumed to result in a less predictable dispersion of aluminum. Strength was also found to decrease with increasing tin content, with pure aluminum generally having the highest strengths. This trend in strength, along with the post-heating gaps in the aluminum and tin interfaces apparent in the SEM images, suggests that tin is in fact a poor binder for aluminum. Instead, it acts more as a spacer and cushion between aluminum particles, reducing the effective strength of the composite. Consequently, if the desired effect of an RM binder additive is to increase adhesion and structural integrity of pressed aluminum powder, tin is not an ideal material. Rather, tin is more useful if the desired effect is melting induced by impact or explosion to aid in dispersion of the RM. Gas gun testing revealed that samples fragmented with an adequate quantity of particles small enough in diameter to produce a desirable energy release. From the data collected and analyses performed, two Al/Sn formulations (5% and 10% tin with H15 Al, heated for 120 minutes) were down-selected as ideal candidates for further testing and were pressed into small warhead cases.

Based on these results with aluminum and tin, some preliminary work was done on an alternative formulation, consisting of an aluminum and magnesium (Mg) RM powder mixture with zinc (Zn) powder as a replacement for tin. Initial results with 50% Al/Mg and 50% Zn by mass show that pressing this mixture in a CIP is slightly more challenging and results in moderately higher porosity (around 7%) than the Al/Sn samples (around 3%). Nonetheless, this mixture has shown to be safe to work with and further testing will be needed to determine mechanical and physical properties to compare with the Al/Sn samples.

Explosive testing of the pressed warhead cases will be necessary to determine how the tin-aluminum interfaces will be affected under conditions in which the tin is allowed to

melt. In addition to testing the Al/Sn samples already created and the Al/Mg/Zn samples, exploring other alternatives to tin as aluminum additives, such as zirconium (Zr), may lead to even more useful insights to compare with data collected for Al/Sn composites and determine the most effective way to enhance the lethality of RM-cased warheads.

APPENDIX A. HOPKINSON BAR TEST IMAGE SEQUENCES

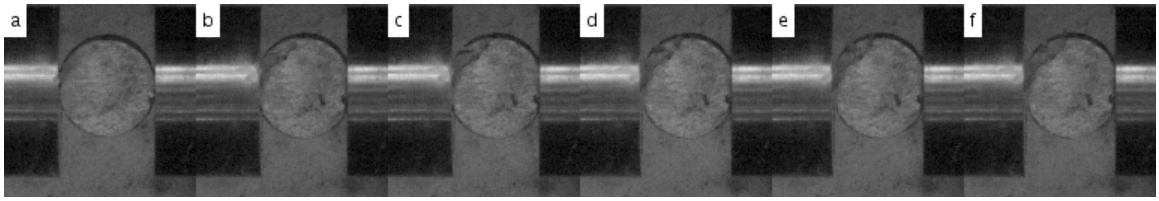

Figure 47. Pure H15 heated for 30 minutes (Brazilian test).

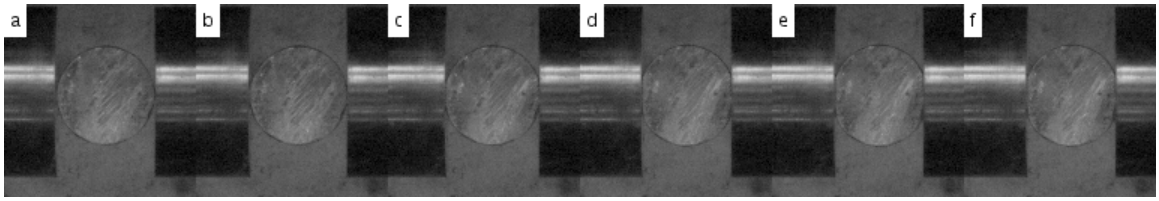

Figure 48. Pure H15 heated for 120 minutes (Brazilian test).

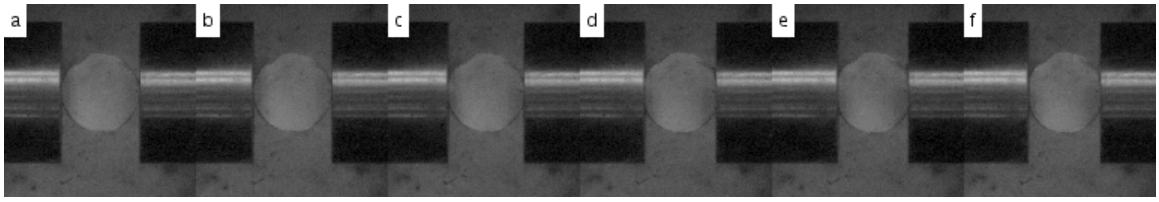

Figure 49. Pure H2 heated for 30 minutes (Brazilian test).

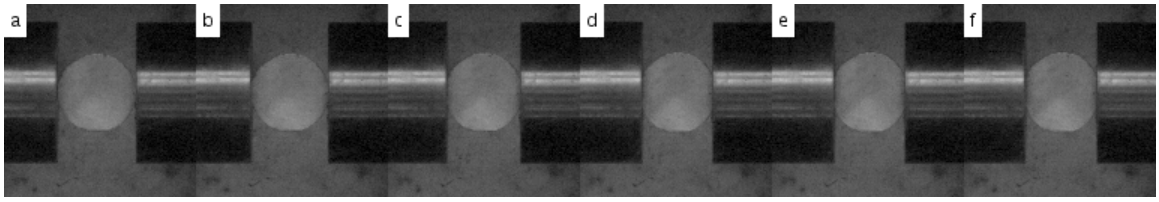

Figure 50. Pure H2 heated for 120 minutes (Brazilian test).

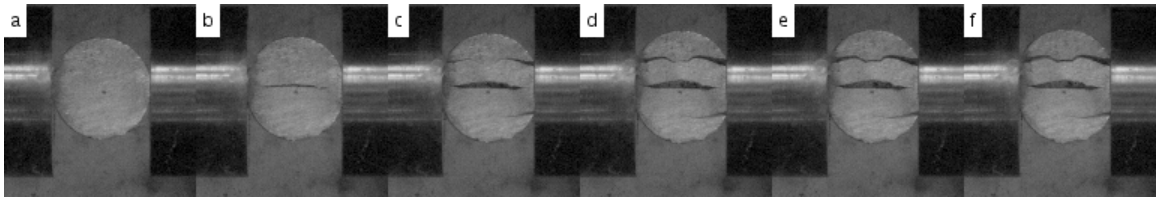

Figure 51. 5% Sn (H15) heated for 30 minutes (Brazilian test).

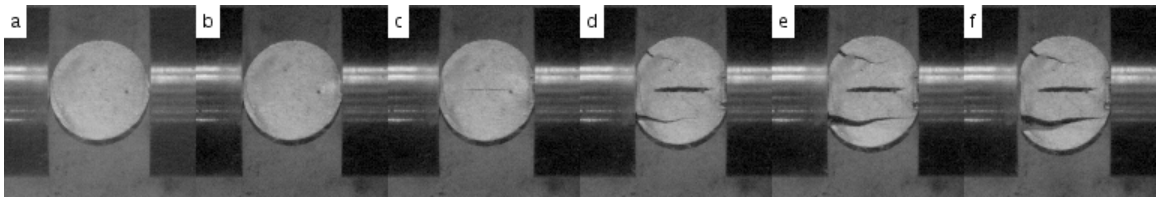

Figure 52. 5% Sn (H15) heated for 120 minutes (Brazilian test).

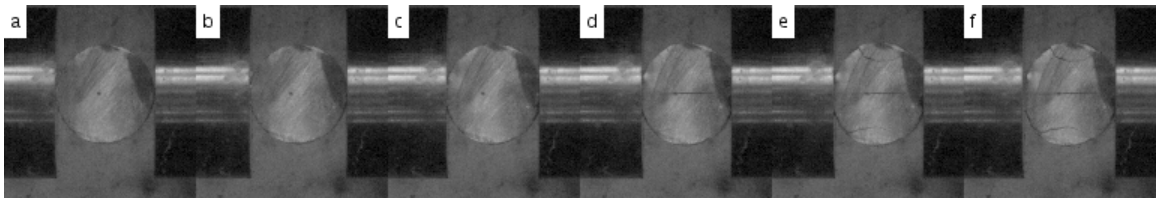

Figure 53. 5% Sn (H2) heated for 30 minutes (1) (Brazilian test).

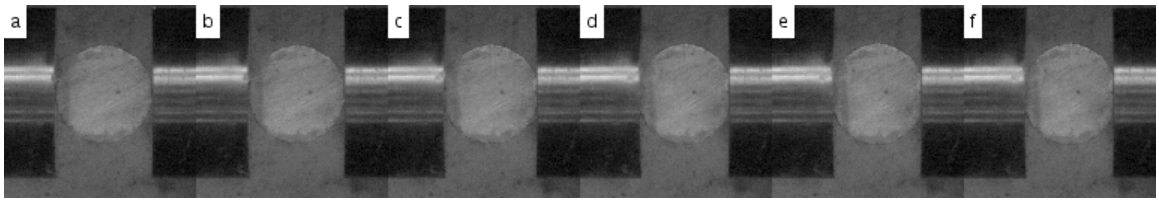

Figure 54. 5% Sn (H2) heated for 120 minutes (1) (Brazilian test).

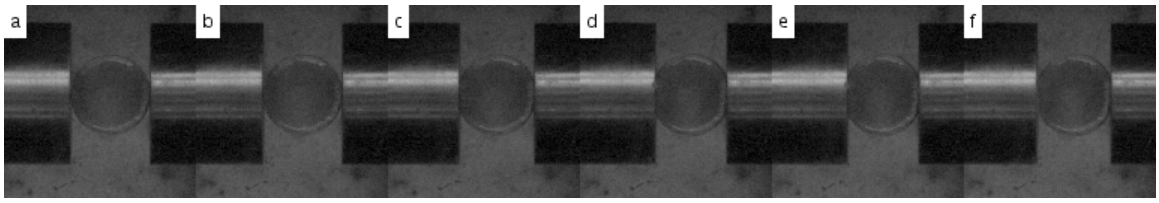

Figure 55. 5% Sn (H2) heated for 30 minutes (2) (Brazilian test).

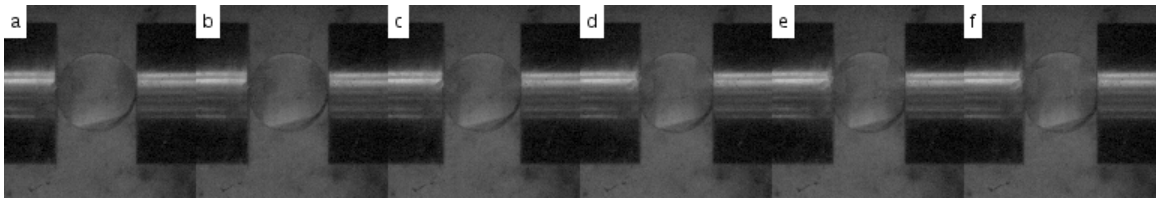

Figure 56. 5% Sn (H2) heated for 120 minutes (2) (Brazilian test).

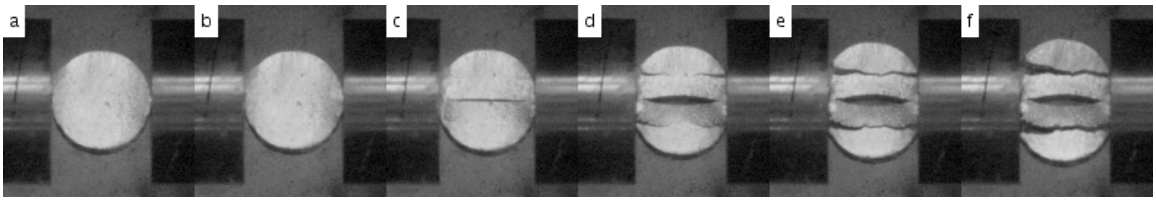

Figure 57. 7.5% Sn (H15) heated for 30 minutes (Brazilian test).

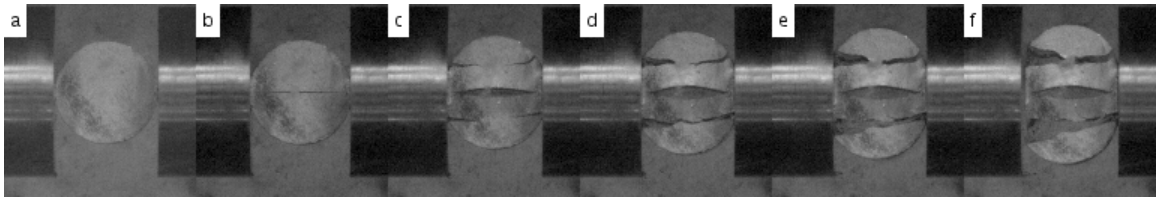

Figure 58. 7.5% Sn (H15) heated for 120 minutes (Brazilian test).

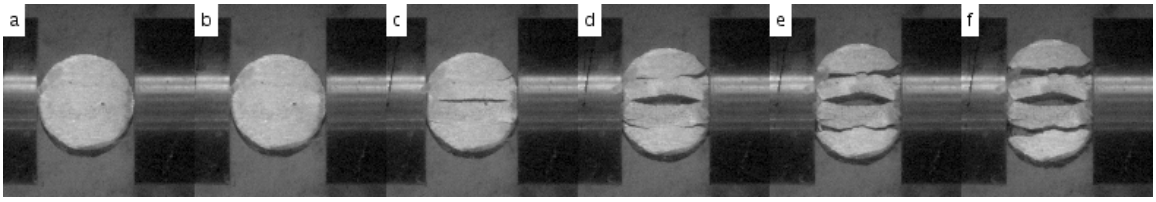

Figure 59. 10% Sn (H15) heated for 30 minutes (Brazilian test).

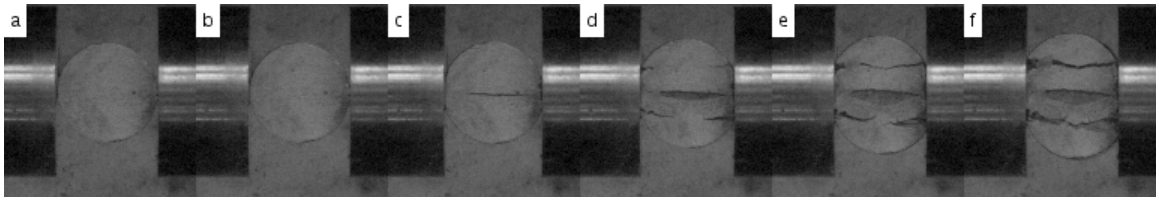

Figure 60. 10% Sn (H15) heated for 120 minutes (Brazilian test).

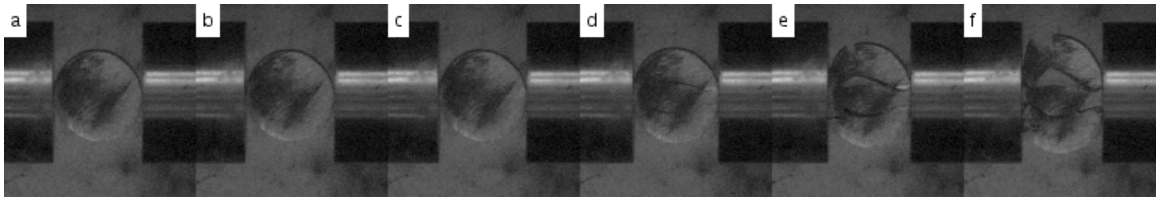

Figure 61. 25% Sn (H15) heated for 30 minutes (Brazilian test).

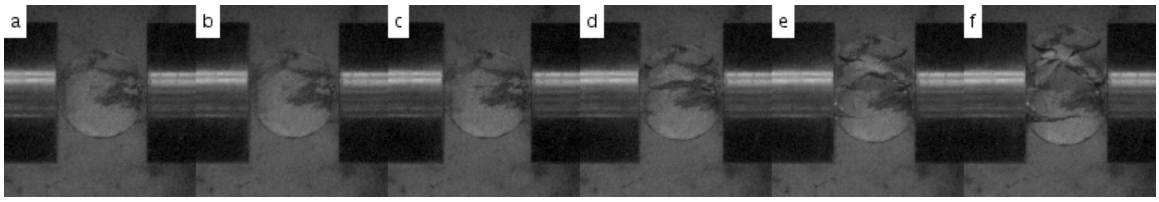

Figure 62. 25% Sn (H15) heated for 120 minutes (Brazilian test).

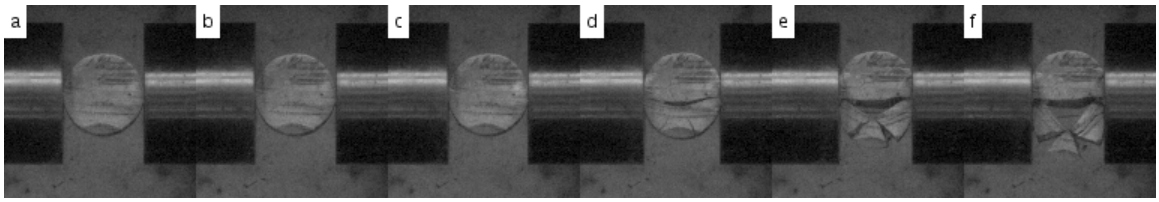

Figure 63. 25% Sn (H2) heated for 30 minutes (Brazilian test).

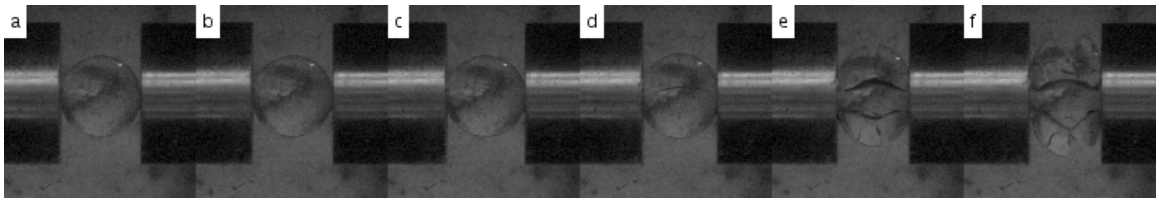

Figure 64. 25% Sn (H2) heated for 120 minutes (Brazilian test).

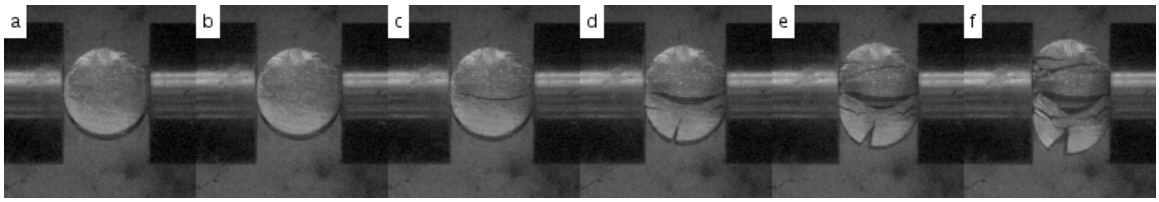

Figure 65. 50% Sn (H15) heated for 5 minutes (Brazilian test).

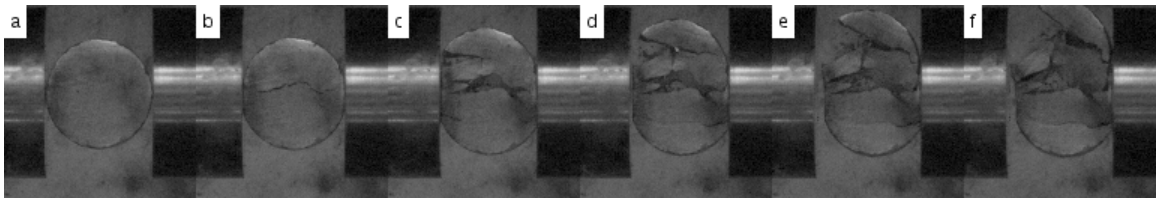

Figure 66. 50% Sn (H15) heated for 30 minutes (Brazilian test).

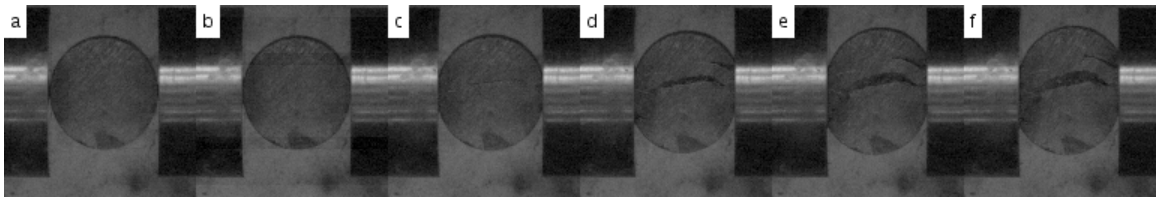

Figure 67. 50% Sn (H15) heated for 120 minutes (Brazilian test).

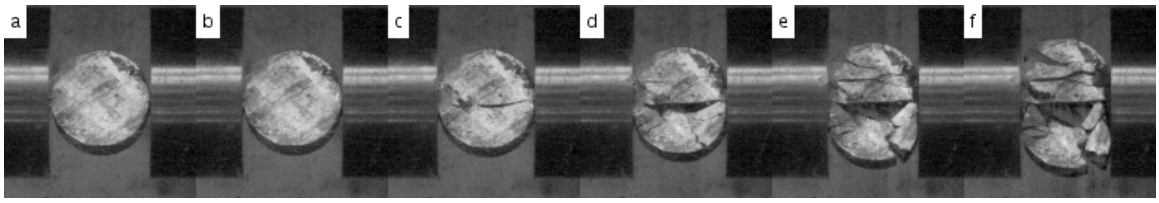

Figure 68. 50% Sn (H2) heated for 30 minutes (Brazilian test).

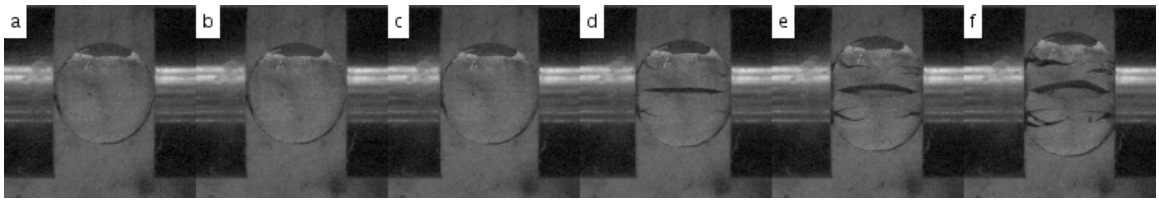

Figure 69. 50% Sn (H2) heated for 120 minutes (Brazilian test).

THIS PAGE INTENTIONALLY LEFT BLANK

APPENDIX B. SEM IMAGES

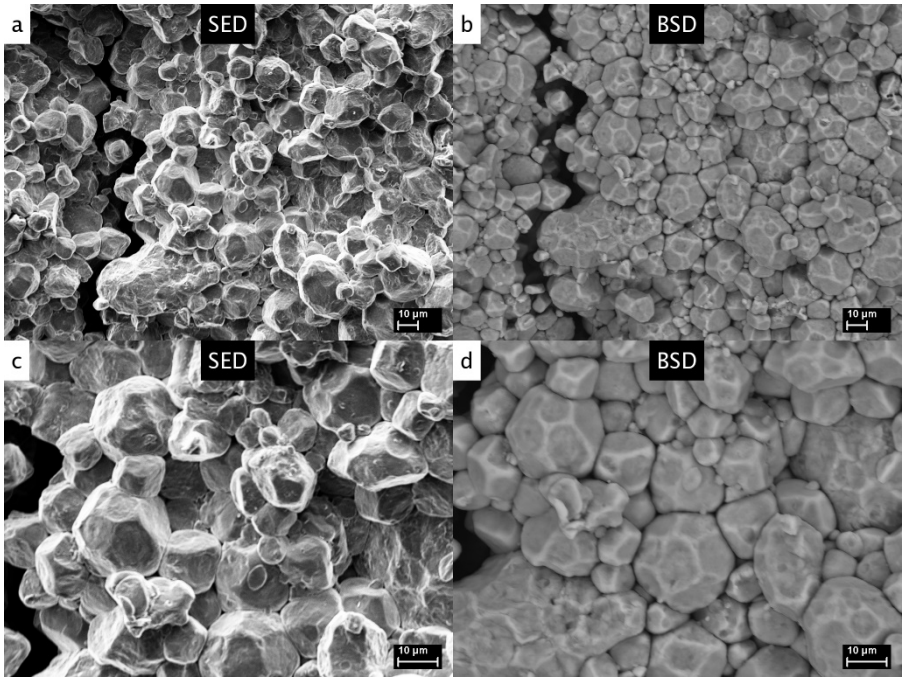

Figure 70. Pure H15 heated for 30 minutes.

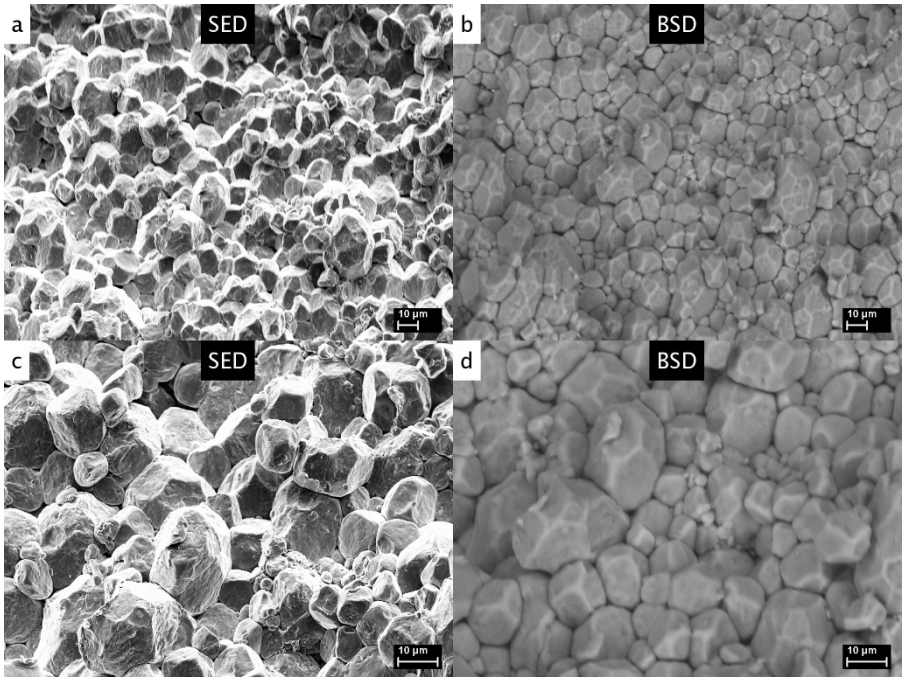

Figure 71. Pure H15 heated for 120 minutes.

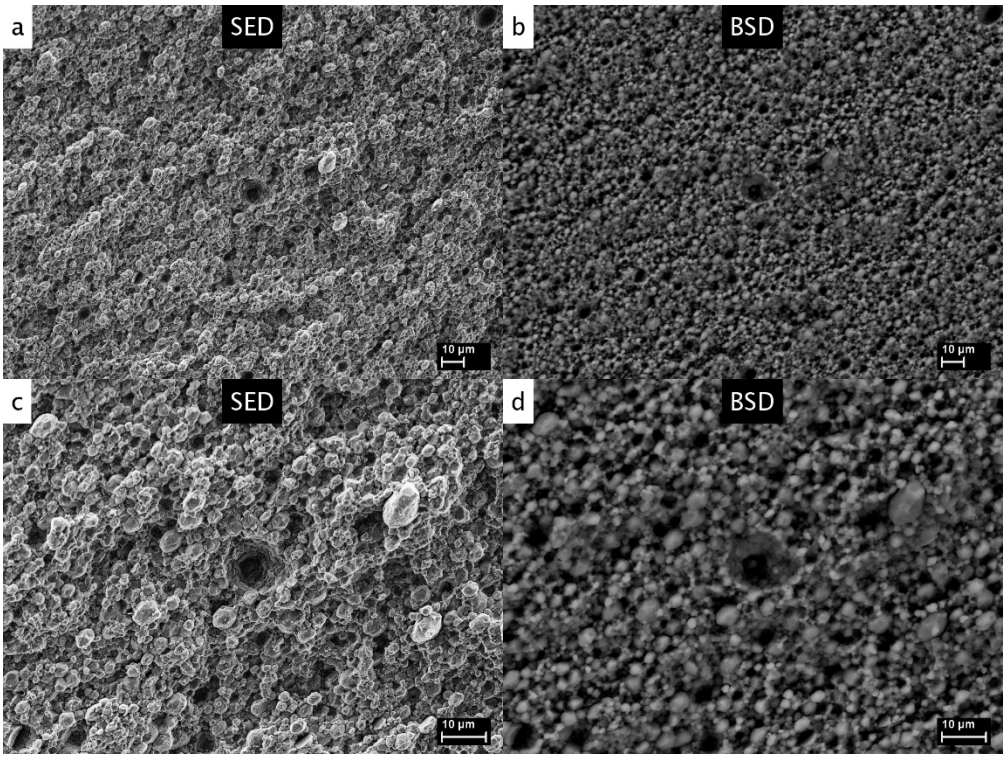

Figure 72. Pure H2 heated for 30 minutes.

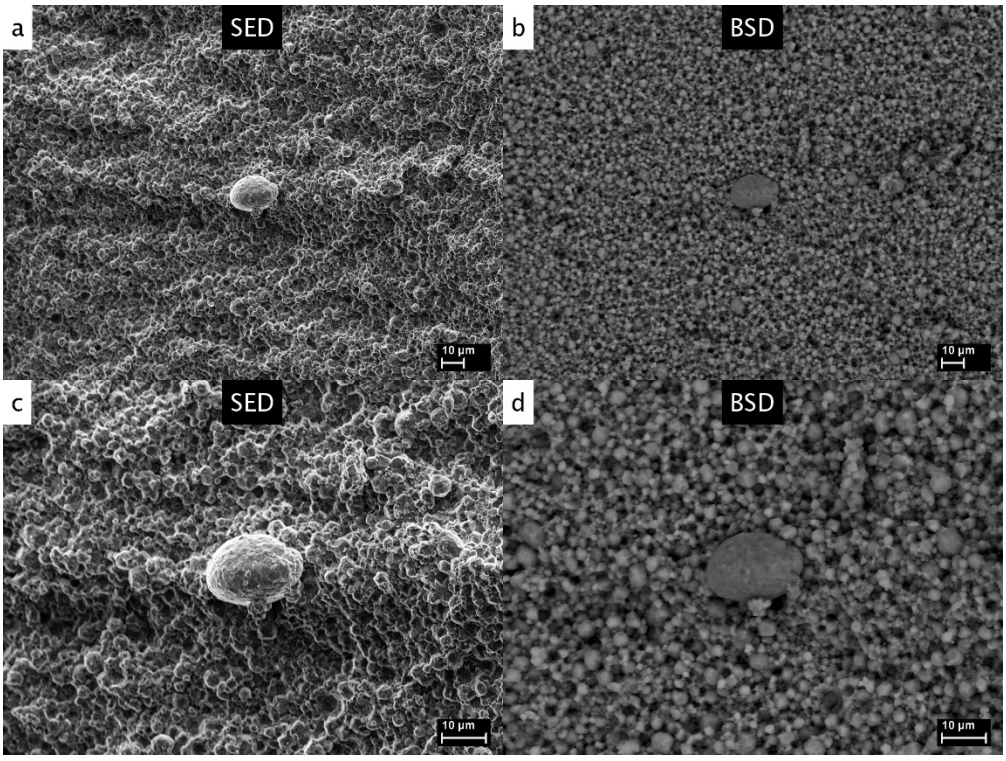

Figure 73. Pure H2 heated for 120 minutes.

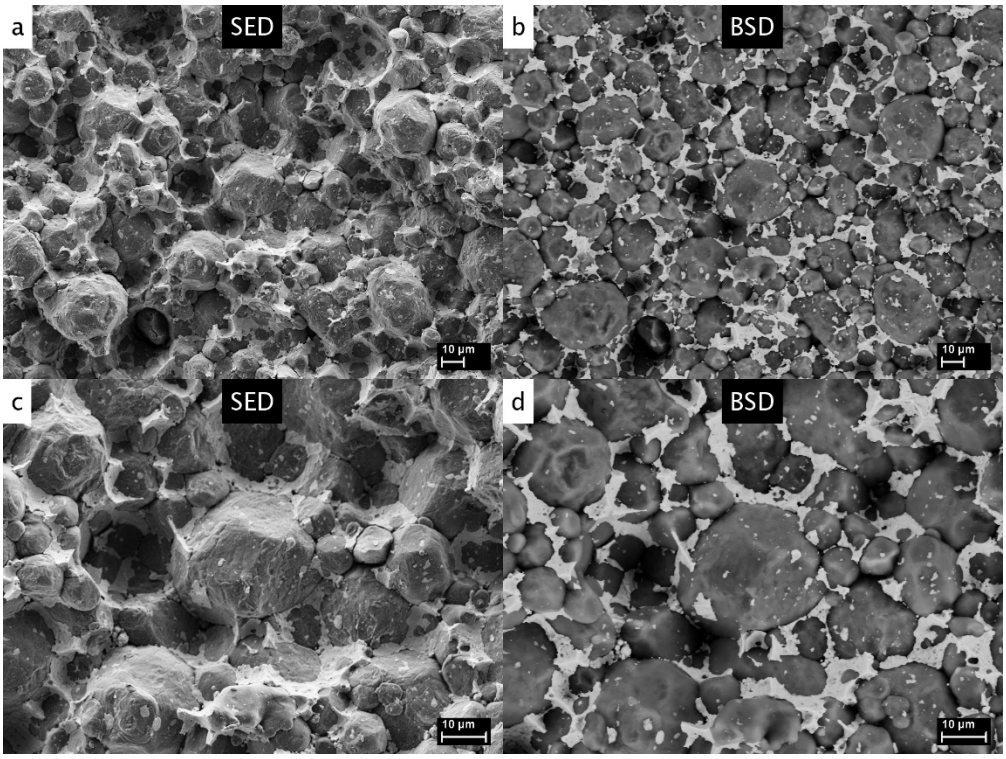

Figure 74. 5% Sn (H15) heated for 30 minutes.

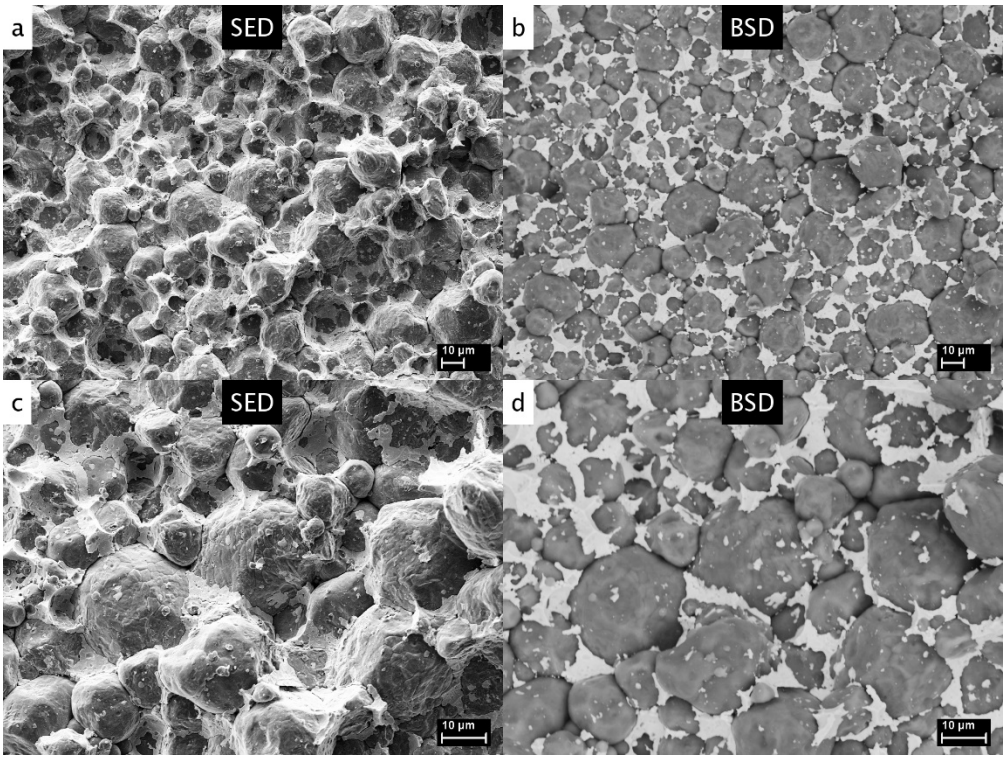

Figure 75. 5% Sn (H15) heated for 120 minutes.

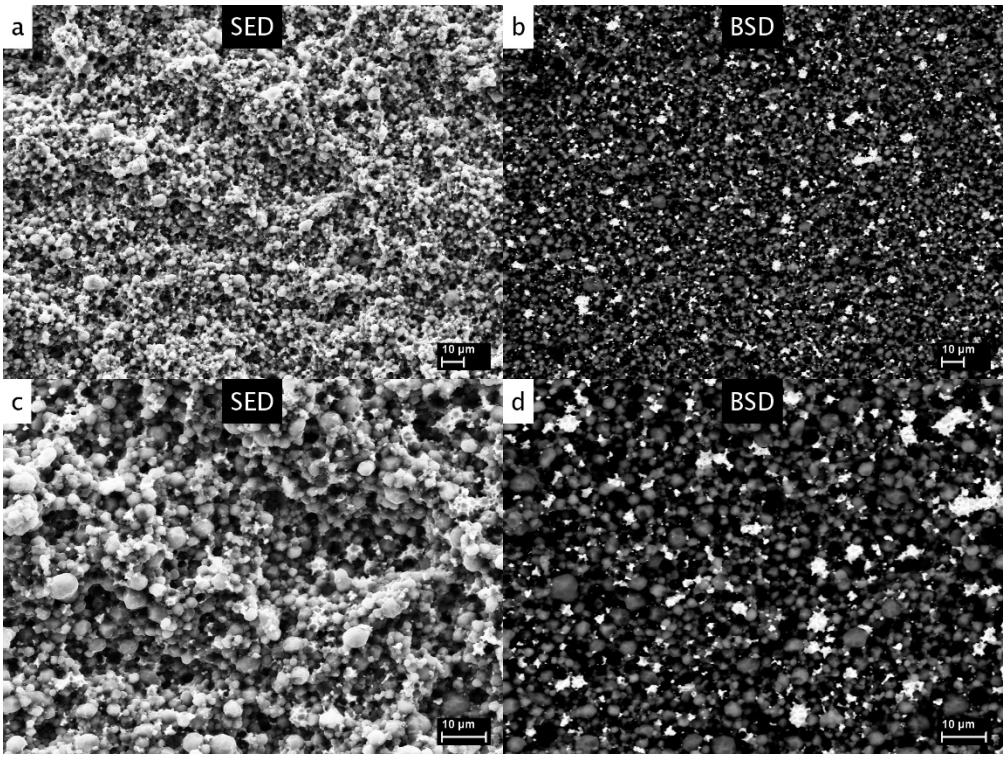

Figure 76. 5% Sn (H2) heated for 30 minutes (1).

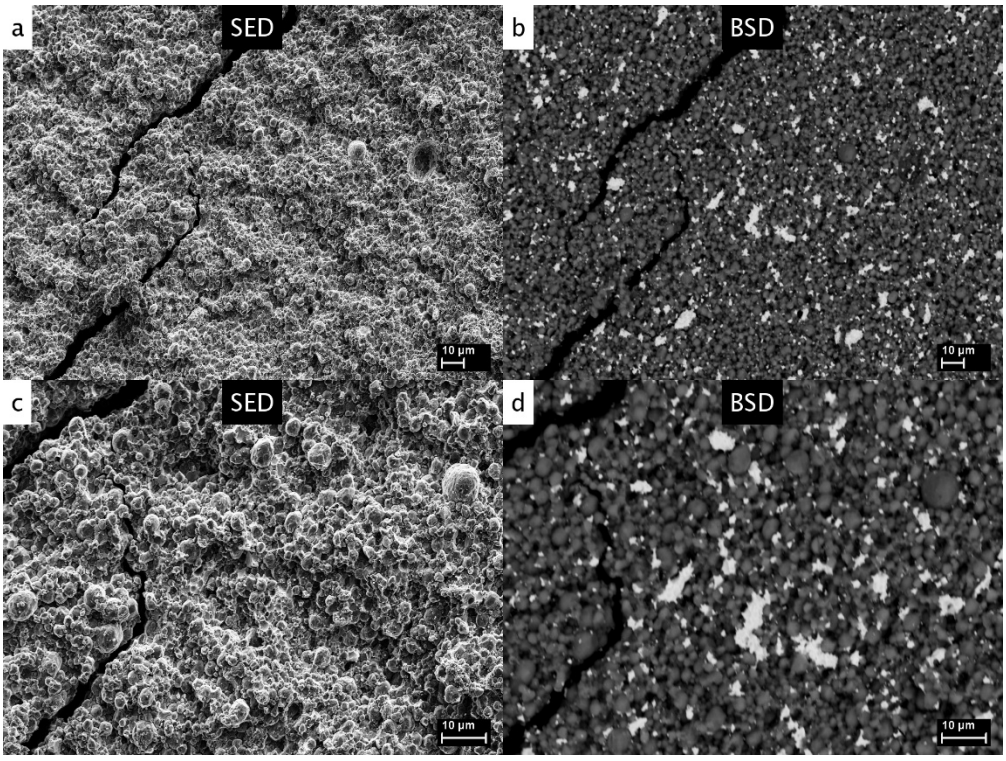

Figure 77. 5% Sn (H2) heated for 120 minutes (1).

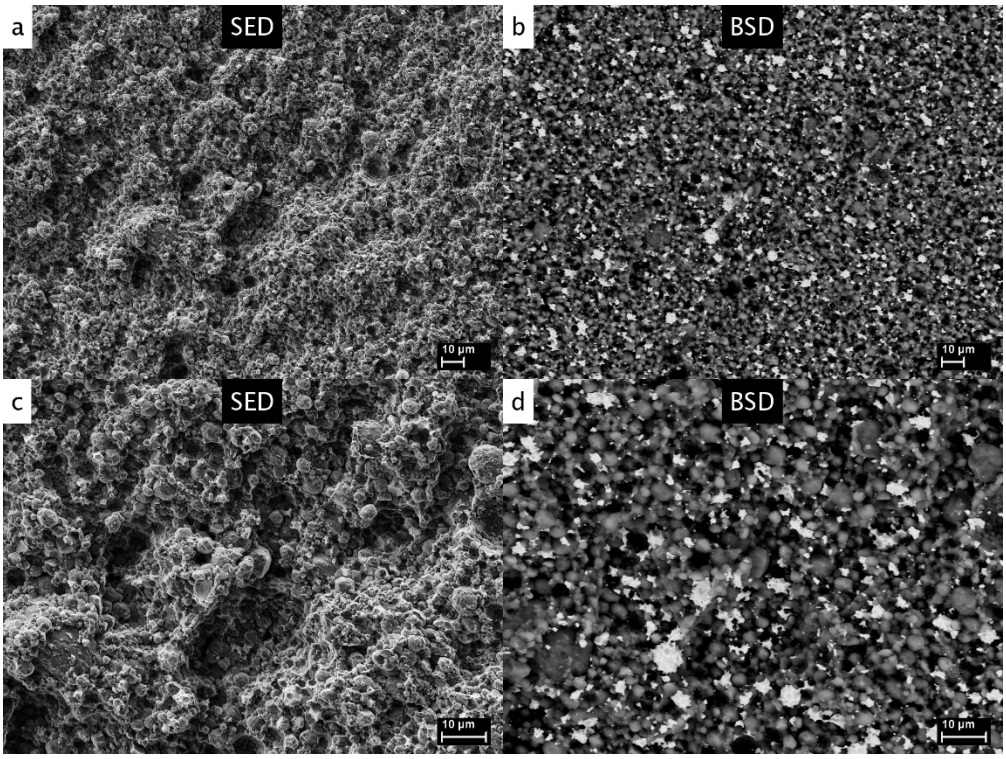

Figure 78. 5% Sn (H2) heated for 30 minutes (2).

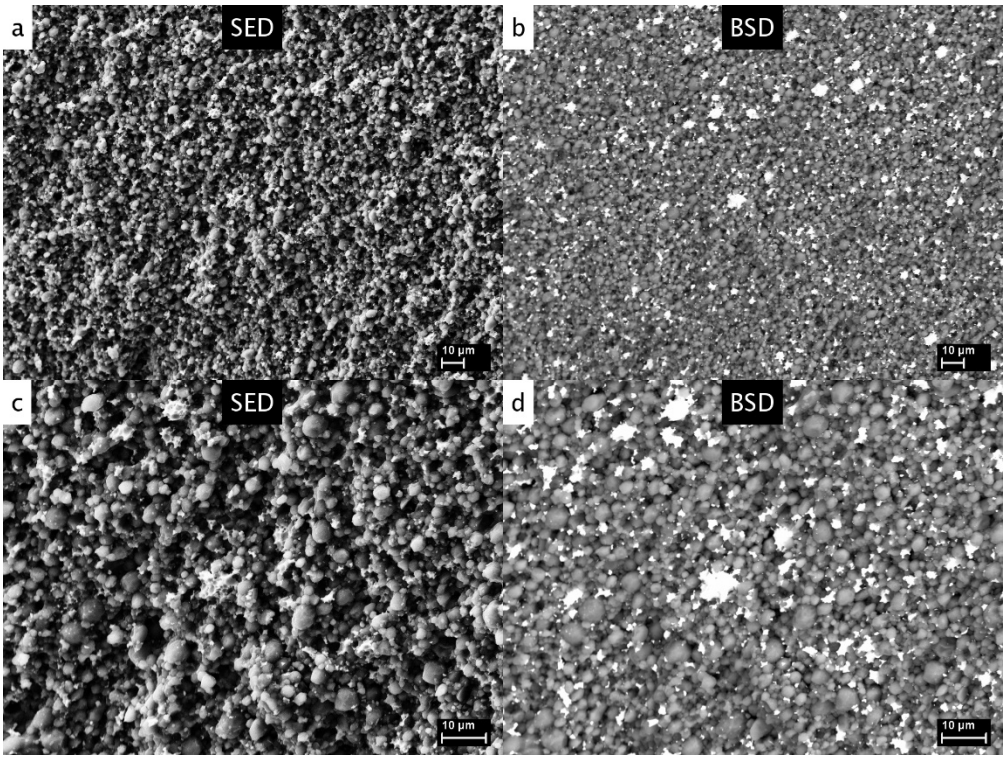

Figure 79. 5% Sn (H2) heated for 120 minutes (2).

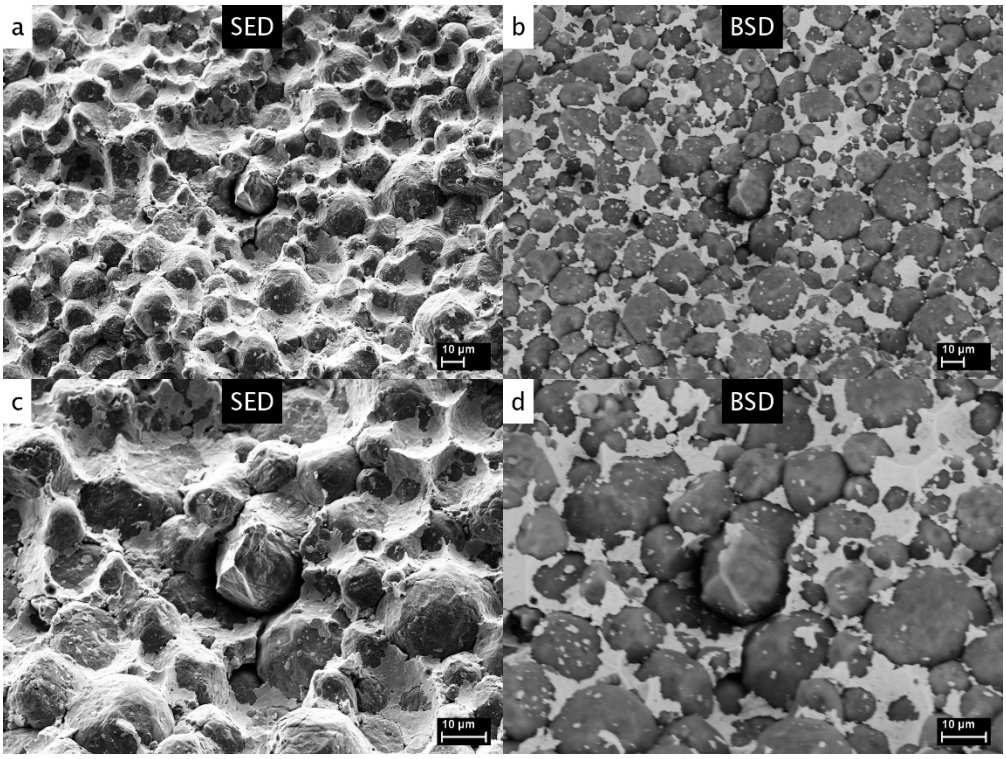

Figure 80. 7.5% Sn (H15) heated for 30 minutes.

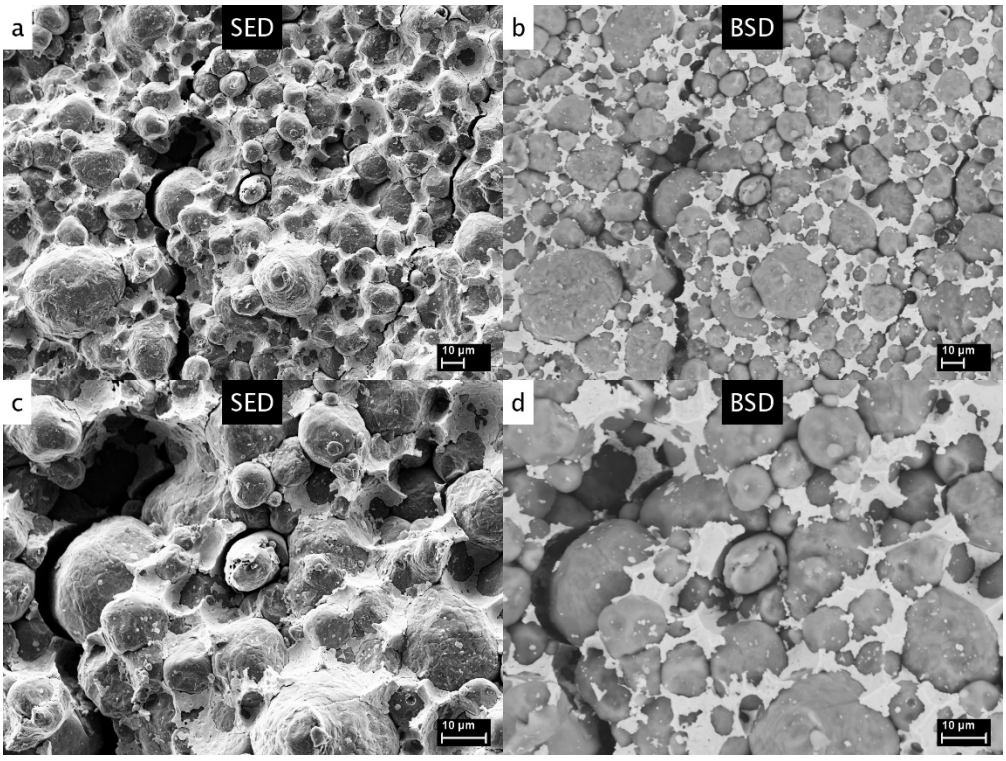

Figure 81. 7.5% Sn (H15) heated for 120 minutes.

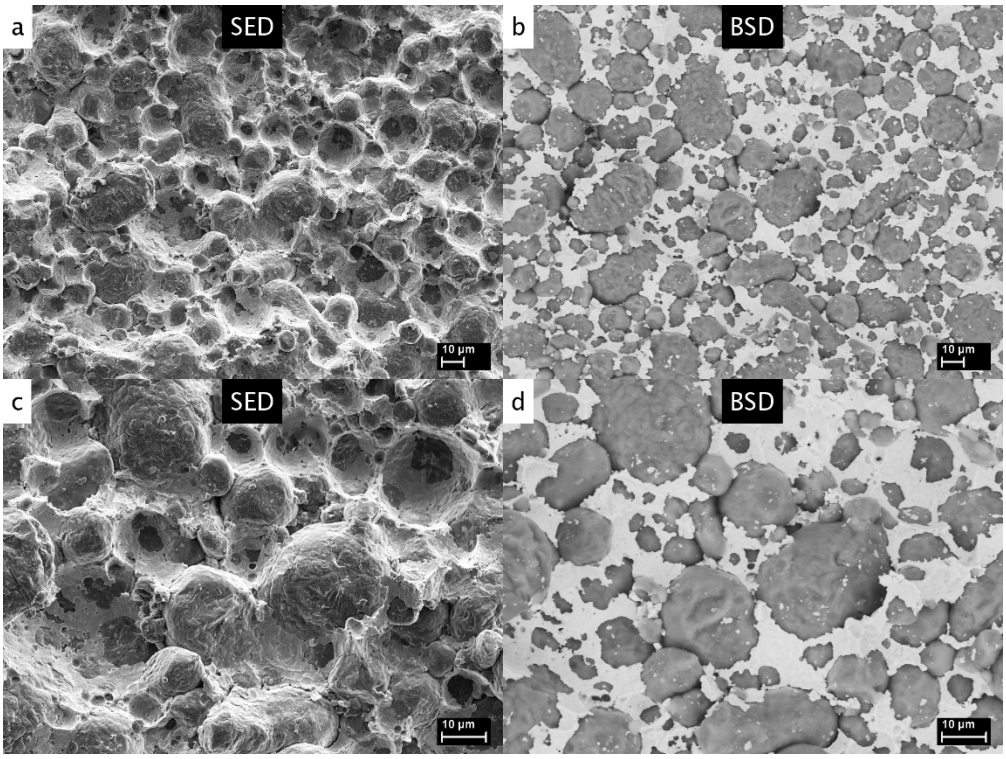

Figure 82. 10% Sn (H15) heated for 30 minutes.

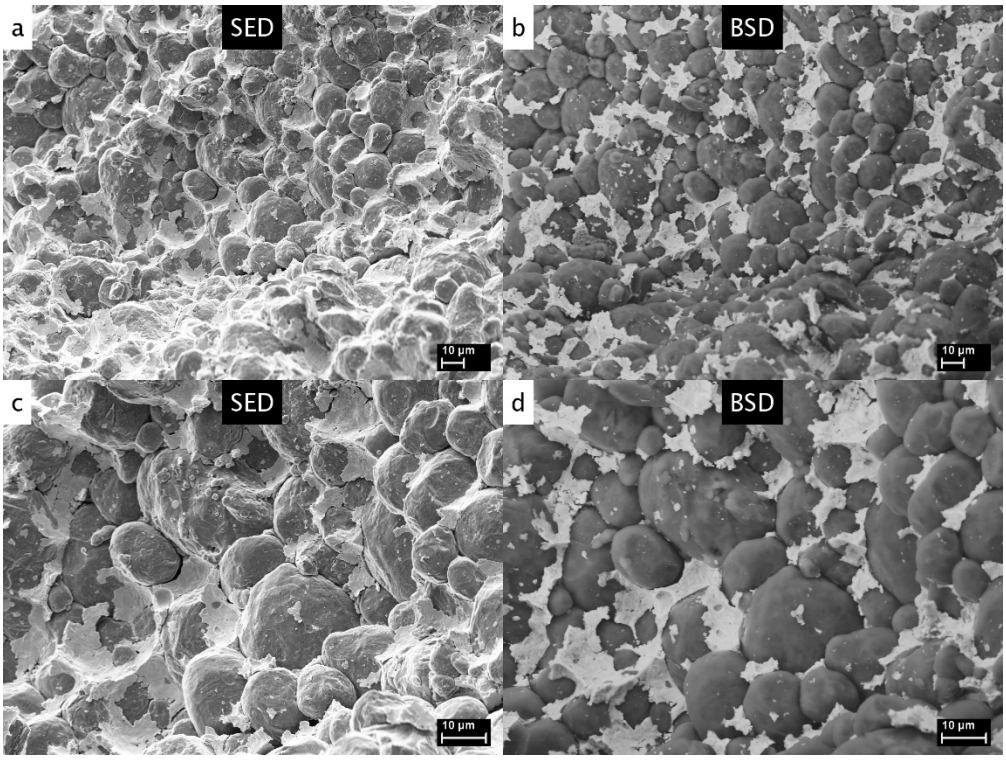

Figure 83. 10% Sn (H15) heated for 120 minutes.

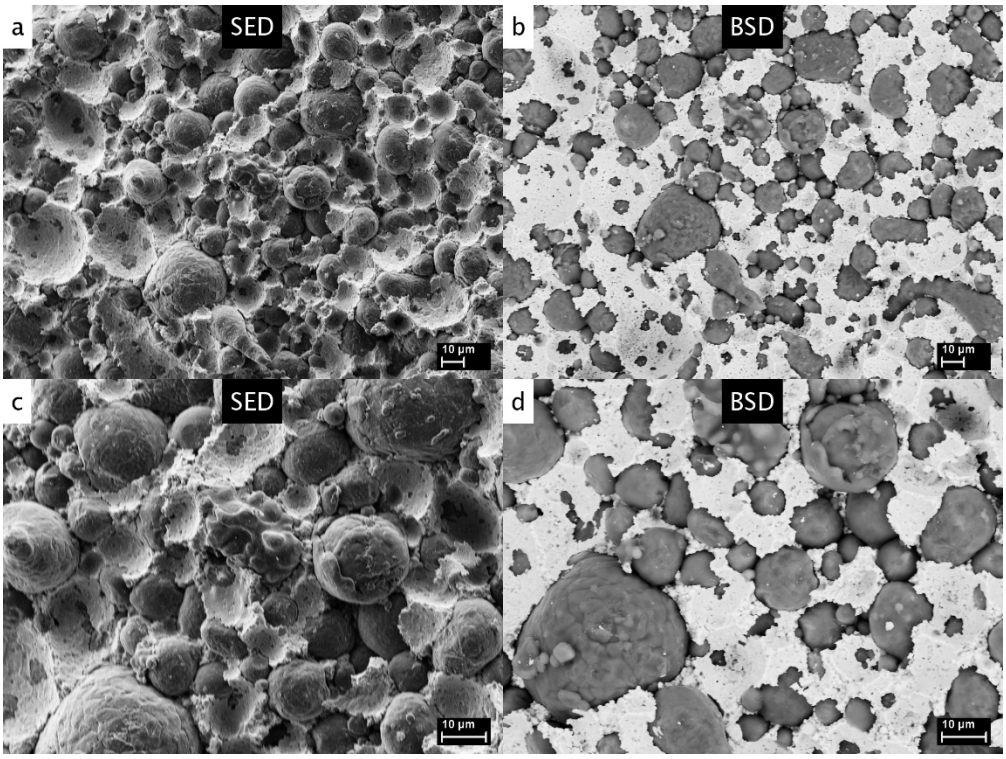

Figure 84. 25% Sn (H15) heated for 30 minutes.

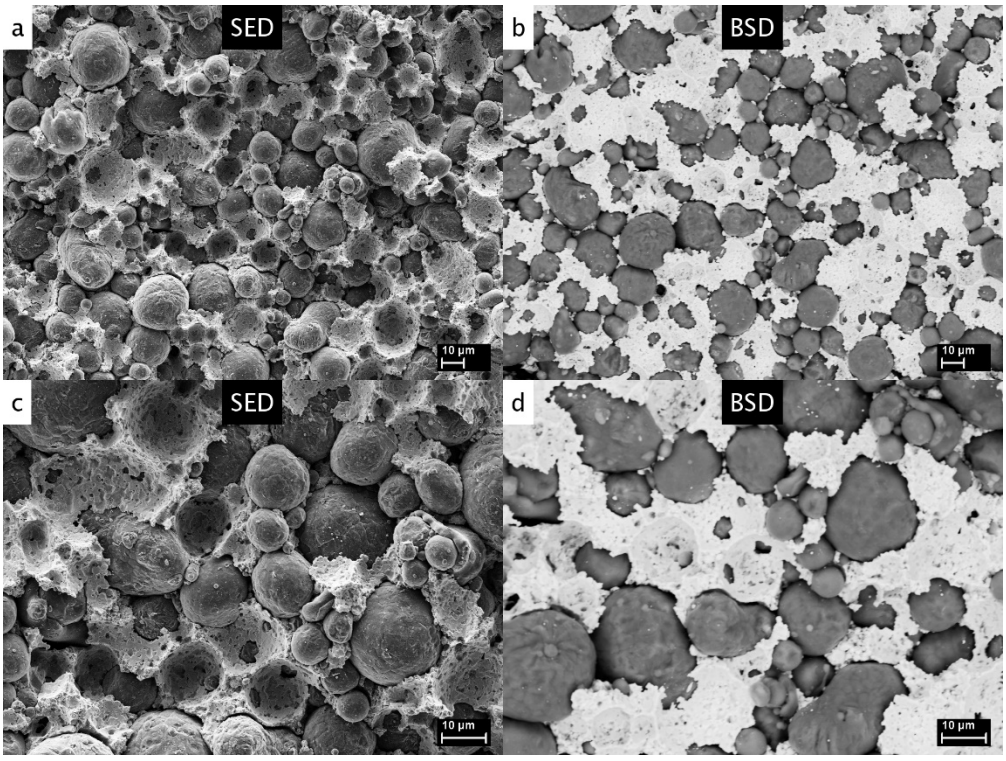

Figure 85. 25% Sn (H15) heated for 120 minutes.

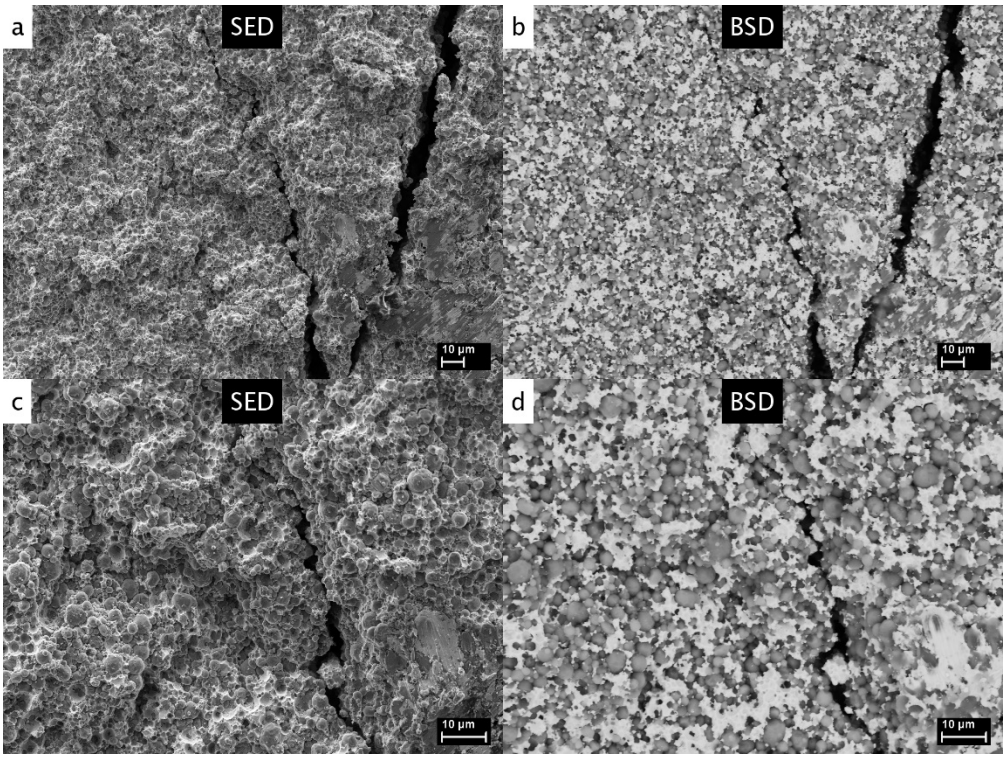

Figure 86. 25% Sn (H2) heated for 30 minutes.

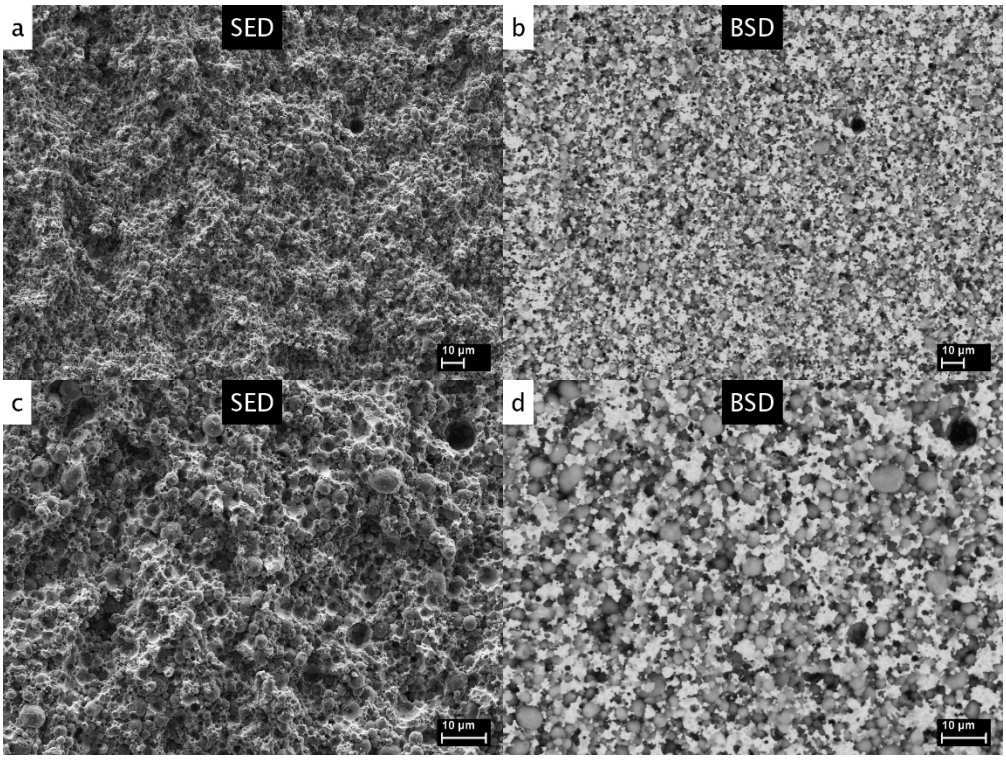

Figure 87. 25% Sn (H2) heated for 120 minutes.

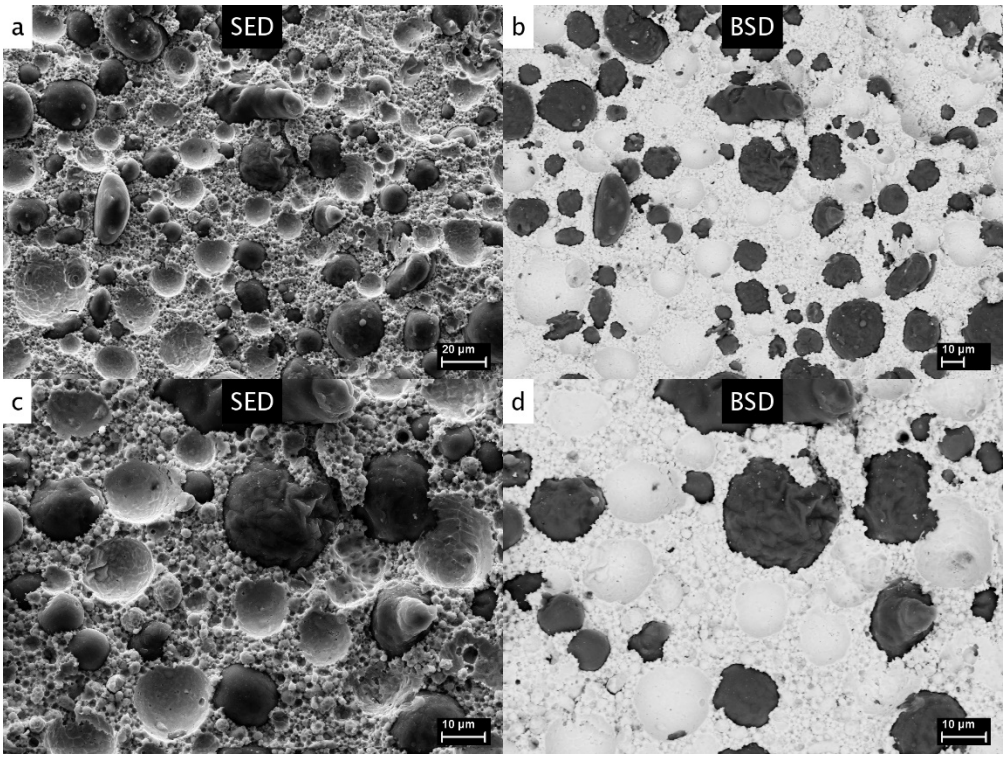

Figure 88. 50% Sn (H15) heated for 5 minutes.

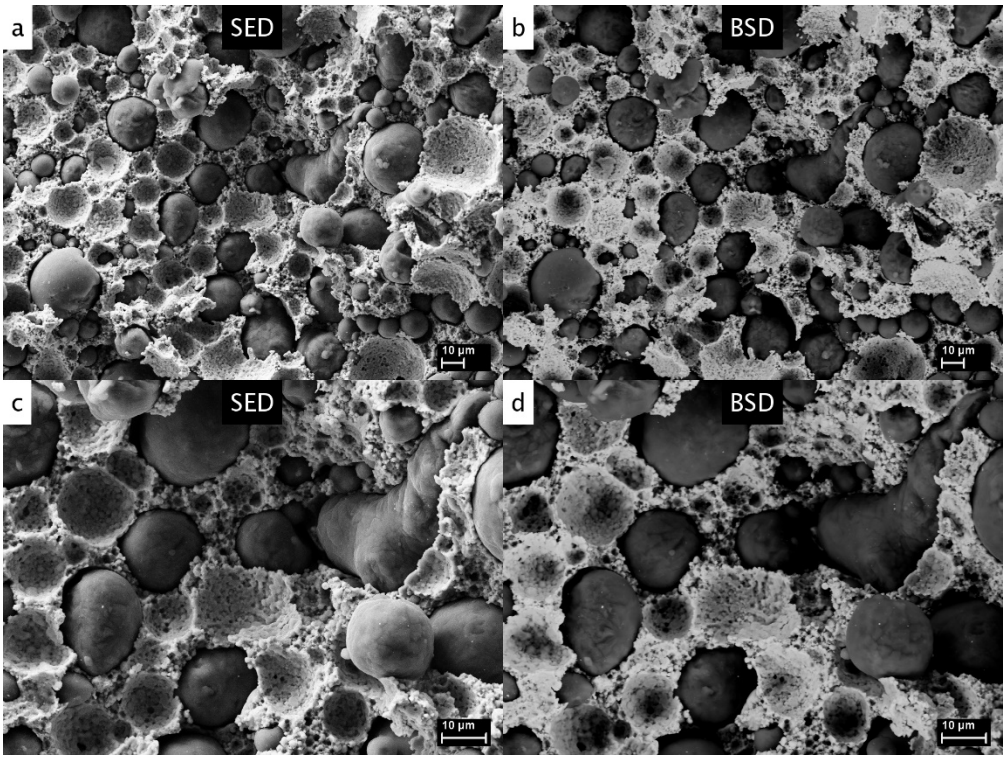

Figure 89. 50% Sn (H15) heated for 30 minutes.

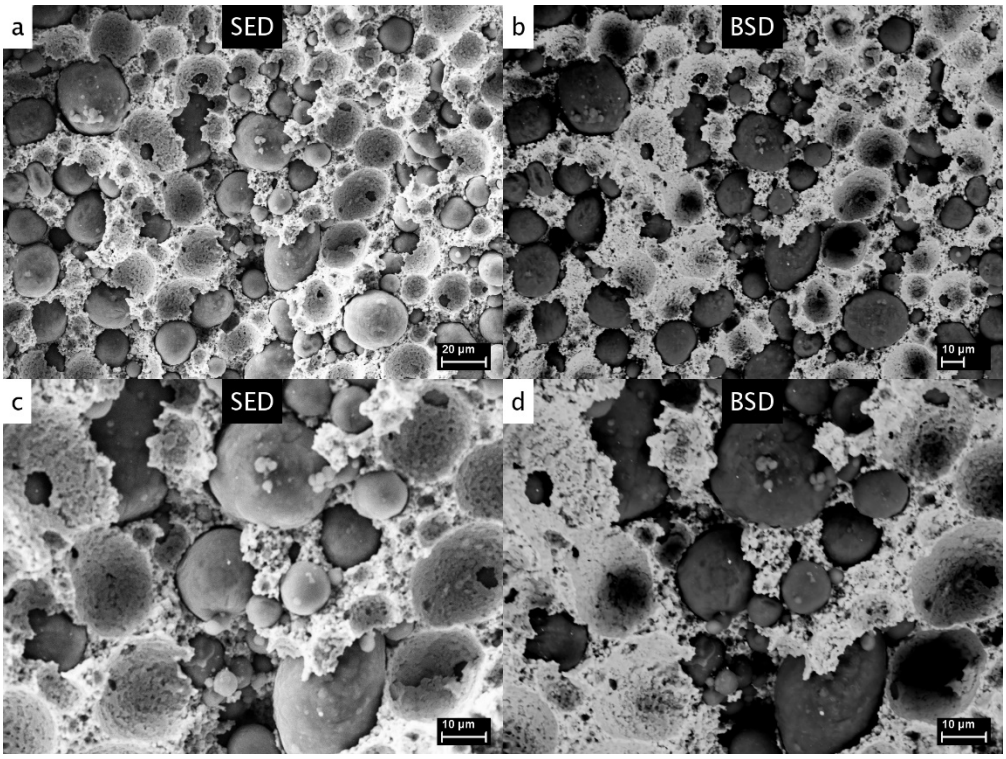

Figure 90. 50% Sn (H15) heated for 120 minutes.

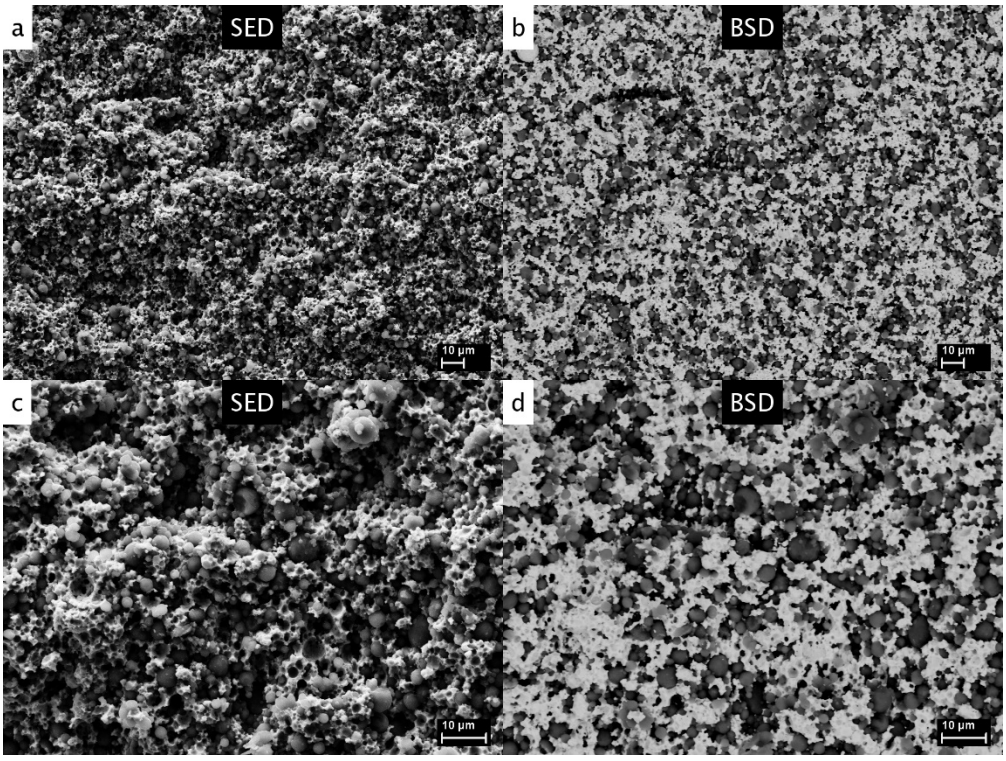

Figure 91. 50% Sn (H2) heated for 30 minutes.

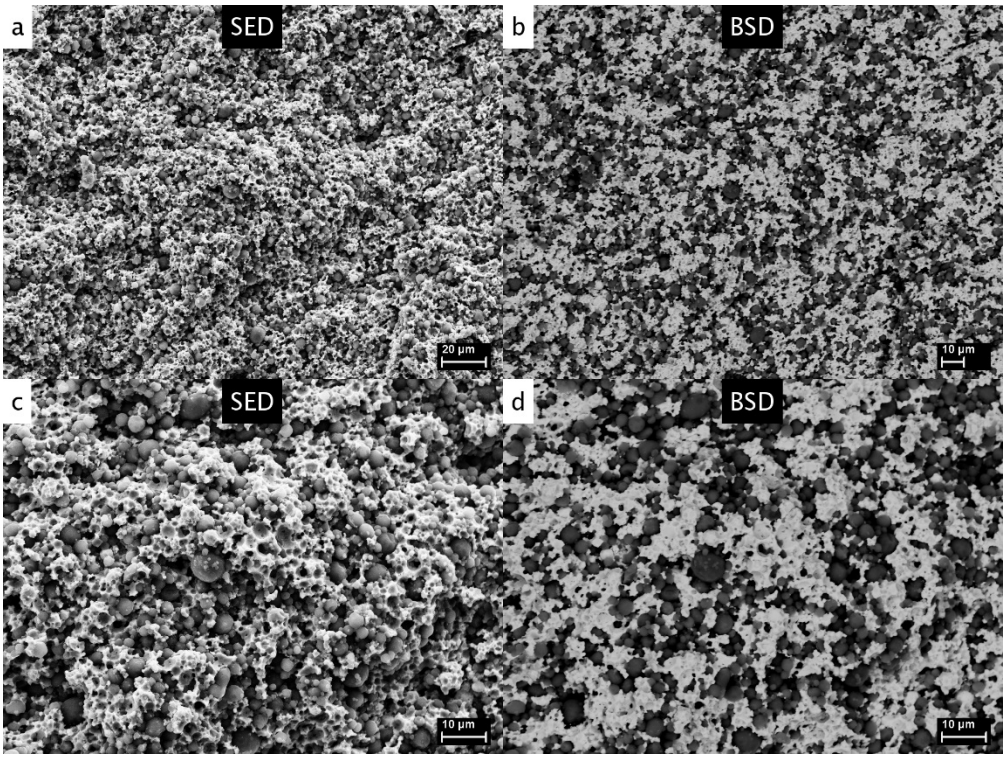

Figure 92. 50% Sn (H2) heated for 120 minutes.

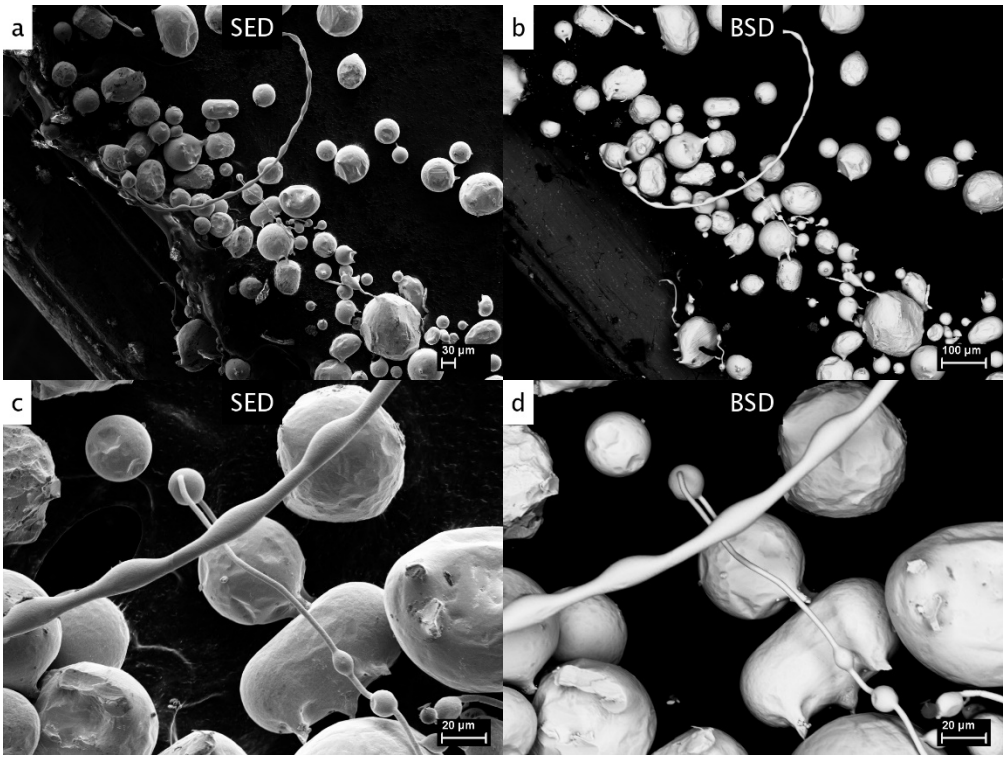

Figure 93. Exuded tin and tin oxides (1).

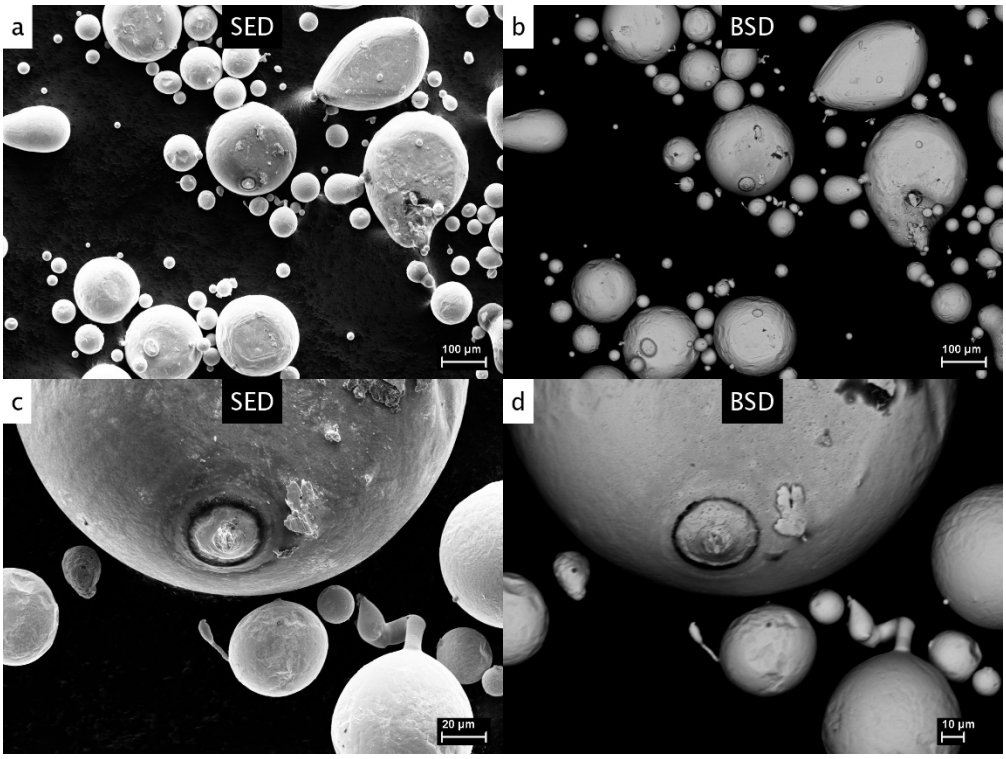

Figure 94. Exuded tin and tin oxides (2).

THIS PAGE INTENTIONALLY LEFT BLANK

APPENDIX C. SAMPLE DATA

Table 10. Porosity calculations.

Sample	Tin Content (% volume)	Heat Duration (min)	TMD (g/cc)	Porosity before heating	Porosity after heating	Change in porosity
0V1B1	0.00%	0	2.705	4.84%	-	-
0V1B2	0.00%	0	2.705	6.05%	-	-
0V1B3	0.00%	30	2.705	4.52%	5.13%	13.46%
0V1B4	0.00%	120	2.705	6.64%	6.90%	3.89%
0V1B5	0.00%	30	2.705	3.21%	3.17%	-1.30%
0V1B6	0.00%	120	2.705	3.43%	3.43%	0.26%
0V1B7	0.00%	0	2.705	4.43%	-	-
0V1B8	0.00%	0	2.705	2.97%	-	-
0V1B9	0.00%	30	2.705	6.63%	6.86%	3.47%
0VH2B1	0.00%	30	2.705	-	5.86%	-
0VH2B2	0.00%	120	2.705	-	6.01%	-
0VH2B3	0.00%	30	2.705	-	5.90%	-
0VH2B4	0.00%	120	2.705	-	5.31%	-
5M1A1	1.91%	120*	2.793	2.20%	2.55%	15.93%
5M1A2	1.91%	120*	2.793	1.72%	2.23%	29.35%
5M1A3	1.91%	120*	2.793	1.49%	1.52%	2.18%
5M1A4	1.91%	120*	2.793	1.85%	1.97%	6.82%
5M1B1	1.91%	120*	2.793	1.62%	1.94%	19.82%
5M1B2	1.91%	120*	2.793	2.01%	2.41%	19.76%
5M1B3	1.91%	120*	2.793	1.79%	2.15%	20.39%
5M1B4	1.91%	120*	2.793	7.47%	7.16%	-4.17%
5M1B5	1.91%	120*	2.793	3.26%	3.24%	-0.54%
5M2A1	1.91%	120*	2.793	3.80%	3.64%	-4.20%
5M2A2	1.91%	120*	2.793	2.03%	2.64%	29.75%
5M2A3	1.91%	120*	2.793	2.15%	2.41%	11.90%
5M2A4	1.91%	120*	2.793	1.64%	2.06%	25.48%
5M2A5	1.91%	120*	2.793	1.76%	2.20%	24.94%
5M2B1	1.91%	120*	2.793	2.15%	3.05%	41.88%
5M2B2	1.91%	120*	2.793	2.36%	2.42%	2.54%
5M2B3	1.91%	120*	2.793	1.61%	2.21%	37.38%
5M2B4	1.91%	120*	2.793	1.82%	2.43%	33.26%
5M2B5	1.91%	120*	2.793	1.99%	2.55%	28.68%
5M3A1	1.91%	120*	2.793	1.65%	2.10%	27.77%
5M3A2	1.91%	120*	2.793	1.30%	-	-
5M3A3	1.91%	120*	2.793	2.06%	2.60%	26.27%
5M3A4	1.91%	120*	2.793	2.87%	2.91%	1.12%
5M3A5	1.91%	120*	2.793	2.08%	2.60%	25.17%
5M3B1	1.91%	120*	2.793	1.94%	-	-
5M3B2	1.91%	120*	2.793	1.93%	-	-
5M3B3	1.91%	120*	2.793	2.66%	2.66%	-0.18%
5M3B4	1.91%	120*	2.793	2.20%	-	-
5M3B5	1.91%	120*	2.793	2.38%	3.18%	33.36%
10M1A1	3.97%	120*	2.888	2.90%	3.25%	11.77%
10M1A2	3.97%	120*	2.888	1.74%	2.76%	58.43%
10M1A3	3.97%	120*	2.888	1.90%	3.36%	76.82%
10M1A4	3.97%	120*	2.888	2.01%	3.23%	60.60%
10M1A5	3.97%	120*	2.888	2.90%	3.20%	10.13%
10M1B1	3.97%	120*	2.888	2.29%	3.76%	63.83%
10M1B2	3.97%	120*	2.888	2.56%	4.11%	60.95%
10M1B3	3.97%	120*	2.888	2.59%	4.30%	66.36%
10M1B4	3.97%	120*	2.888	2.40%	4.17%	73.39%
10M1B5	3.97%	120*	2.888	3.13%	4.82%	53.71%
5V1A1	5.00%	120*	2.935	2.74%	-	-
5V1A2	5.00%	120*	2.935	4.34%	-	-
5V1A3	5.00%	120*	2.935	2.17%	-	-
5V1A4	5.00%	120*	2.935	2.83%	-	-
5V1A5	5.00%	120*	2.935	4.14%	-	-
5V1B1	5.00%	120*	2.935	2.54%	-	-

Sample	Tin Content (% volume)	Heat Duration (min)	TMD (g/cc)	Porosity before heating	Porosity after heating	Change in porosity
5V1B2	5.00%	120*	2.935	2.09%	-	-
5V1B3	5.00%	120*	2.935	2.96%	6.99%	135.72%
5V1B4	5.00%	120*	2.935	2.89%	-	-
5V1B5	5.00%	120*	2.935	4.41%	-	-
5V2B1	5.00%	30	2.935	2.90%	2.68%	-7.60%
5V2B2	5.00%	30	2.935	2.40%	3.06%	27.73%
5V2B3	5.00%	120	2.935	3.40%	3.03%	-10.75%
5V2B4	5.00%	120	2.935	0.92%	0.64%	-30.41%
5V2B5	5.00%	30	2.935	2.16%	2.26%	4.83%
5VH2B1	5.00%	120	2.935	5.06%	5.40%	6.68%
5VH2B2	5.00%	120	2.935	4.64%	4.88%	5.24%
5VH2B3	5.00%	30	2.935	5.82%	5.37%	-7.65%
5VH2B4	5.00%	30	2.935	5.60%	5.87%	4.81%
5VH2B5	5.00%	30	2.935	7.89%	7.31%	-7.37%
5VH2B6	5.00%	120	2.935	5.47%	5.39%	-1.49%
5VH2B7	5.00%	30	2.935	5.92%	6.41%	8.21%
5VH2B8	5.00%	120	2.935	5.20%	5.11%	-1.77%
7.5V1A1	7.50%	120*	3.050	1.79%	-	-
7.5V1A2	7.50%	120*	3.050	2.85%	-	-
7.5V1A3	7.50%	120*	3.050	2.10%	-	-
7.5V1A4	7.50%	0	3.050	1.31%	-	-
7.5V1A5	7.50%	0	3.050	1.92%	-	-
7.5V1B1	7.50%	120*	3.050	1.50%	-	-
7.5V1B2	7.50%	120*	3.050	1.47%	-	-
7.5V1B3	7.50%	120*	3.050	2.13%	-	-
7.5V1B4	7.50%	30	3.050	1.60%	1.76%	10.26%
7.5V1B5	7.50%	30	3.050	1.73%	2.95%	70.75%
7.5V2B1	7.50%	30	3.050	2.77%	2.75%	-1.06%
7.5V2B2	7.50%	120	3.050	2.60%	2.47%	-5.12%
7.5V2B3	7.50%	120	3.050	2.26%	2.14%	-5.35%
10V1A1	10.00%	0	3.166	2.77%	-	-
10V1A2	10.00%	0	3.166	1.69%	-	-
10V1A3	10.00%	0	3.166	3.03%	-	-
10V1A4	10.00%	0	3.166	2.62%	-	-
10V1A5	10.00%	0	3.166	1.67%	-	-
10V1B1	10.00%	30	3.166	1.71%	2.59%	51.94%
10V1B2	10.00%	30	3.166	2.09%	1.95%	-6.65%
10V1B3	10.00%	30	3.166	2.92%	2.91%	-0.36%
10V1B4	10.00%	120	3.166	2.82%	2.72%	-3.52%
10V1B6	10.00%	120	3.166	5.24%	5.72%	9.13%
10V2B1	10.00%	120	3.166	2.11%	2.32%	10.21%
25V1B1	25.00%	30	3.856	2.89%	3.57%	23.24%
25V1B2	25.00%	120	3.856	3.78%	7.66%	102.86%
25V1B3	25.00%	30	3.856	1.95%	3.66%	87.15%
25V1B4	25.00%	120	3.856	1.31%	6.44%	391.39%
25VH2B1	25.00%	30	3.856	3.30%	3.43%	3.99%
25VH2B2	25.00%	120	3.856	3.17%	2.71%	-14.55%
25VH2B3	25.00%	30	3.856	3.09%	3.21%	3.84%
25VH2B4	25.00%	120	3.856	2.70%	2.86%	5.85%
50V1B1	50.00%	30	5.008	4.15%	13.20%	217.78%
50V1B2	50.00%	120	5.008	3.61%	14.71%	307.72%
50V1B3	50.00%	30	5.008	2.99%	8.46%	182.53%
50V1B4	50.00%	120	5.008	3.42%	14.80%	332.16%
50V1B5	50.00%	5	5.008	3.23%	3.08%	-4.76%
50VH2B1	50.00%	30	5.008	3.24%	5.33%	64.30%
50VH2B2	50.00%	120	5.008	4.89%	6.59%	34.85%
50VH2B3	50.00%	30	5.008	3.84%	5.71%	48.78%
50VH2B4	50.00%	120	5.008	4.00%	7.43%	85.54%

* Heated in vacuum drying oven

Table 11. Sample dimensions.

	Before Heating					After Heating					
Sample	l (mm)	d_1 (mm)	d_2 (mm)	d_{avg} (mm)	m (g)	l (mm)	d_1 (mm)	d_2 (mm)	d_{avg} (mm)	m (g)	Duration (min)
0V1B1	5.036	10.843	10.848	10.846	1.1976	-	-	-	-	-	0
0V1B2	5.005	10.899	10.954	10.927	1.1927	-	-	-	-	-	0
0V1B3	5.196	10.854	10.801	10.828	1.2356	5.203	10.806	10.902	10.854	1.2354	30
0V1B4	4.919	10.849	10.855	10.852	1.1490	4.918	10.846	10.878	10.862	1.1477	120
0V1B5	6.675	10.801	10.819	10.810	1.6040	6.674	10.797	10.824	10.8105	1.6046	30
0V1B6	6.355	10.821	10.805	10.813	1.5245	6.356	10.824	10.802	10.813	1.5246	120
0V1B7	6.435	10.840	10.796	10.818	1.5291	-	-	-	-	-	0
0V1B8	5.002	10.850	10.830	10.840	1.2116	-	-	-	-	-	0
0V1B9	5.545	11.171	11.215	11.193	1.3780	5.540	11.214	11.200	11.207	1.3768	30
0VH2B1	-	-	-	-	-	5.520	10.432	10.456	10.444	1.2042	30
0VH2B2	-	-	-	-	-	5.395	10.478	10.533	10.5055	1.1889	120
0VH2B3	-	-	-	-	-	5.078	10.427	10.483	10.455	1.1097	30
0VH2B4	-	-	-	-	-	5.560	10.455	10.381	10.418	1.2140	120
5M1A1	9.792	10.991	11.005	10.998	2.5410	9.798	11.001	11.026	11.0135	2.5406	120*
5M1A2	9.924	11.000	10.980	10.990	2.5840	9.930	11.023	11.005	11.014	2.5835	120*
5M1A3	9.703	10.968	11.015	10.992	2.5332	9.715	10.975	10.995	10.985	2.5325	120*
5M1A4	10.014	11.006	10.883	10.945	2.5826	10.018	11.010	10.887	10.9485	2.5822	120*
5M1B1	4.738	10.949	11.006	10.978	1.2322	4.740	11.060	10.928	10.994	1.2324	120*
5M1B2	4.910	10.881	11.031	10.956	1.2668	4.915	10.894	11.048	10.971	1.2664	120*
5M1B3	5.233	10.864	11.025	10.945	1.3504	5.238	10.868	11.044	10.956	1.3495	120*
5M1B4	4.998	11.510	11.271	11.391	1.3162	4.979	11.511	11.276	11.3935	1.3163	120*
5M1B5	5.565	11.466	11.776	11.621	1.5949	5.569	11.431	11.794	11.6125	1.5940	120*
5M2A1	9.620	11.117	11.144	11.131	2.5149	9.643	11.104	11.112	11.108	2.5149	120*
5M2A2	10.053	10.990	10.900	10.945	2.5880	10.099	11.004	10.903	10.9535	2.5878	120*
5M2A3	10.320	10.979	10.951	10.965	2.6633	10.324	10.986	10.966	10.976	2.6627	120*
5M2A4	10.249	10.950	10.871	10.911	2.6323	10.262	10.965	10.885	10.925	2.6314	120*
5M2A5	9.856	10.915	10.989	10.952	2.5477	9.878	10.928	11.001	10.9645	2.5478	120*
5M2B1	5.092	10.922	10.940	10.931	1.3060	5.120	10.936	10.967	10.9515	1.3060	120*
5M2B2	5.145	10.915	10.895	10.905	1.3105	5.158	10.875	10.915	10.895	1.3106	120*
5M2B3	4.738	10.889	10.882	10.886	1.2117	4.755	10.911	10.887	10.899	1.2116	120*
5M2B4	5.197	10.982	10.987	10.985	1.3505	5.211	10.995	11.010	11.0025	1.3502	120*
5M2B5	5.070	11.006	11.024	11.015	1.3226	5.080	11.026	11.044	11.035	1.3223	120*
5M3A1	10.305	10.966	11.022	10.994	2.6873	10.322	10.977	11.049	11.013	2.6885	120*
5M3A2	10.755	10.912	11.011	10.962	2.7979	-	-	-	-	-	120*
5M3A3	10.373	10.948	10.894	10.921	2.6581	10.349	10.949	10.978	10.9635	2.6579	120*
5M3A4	10.064	10.774	10.983	10.879	2.5375	10.059	10.762	11.001	10.8815	2.5368	120*
5M3A5	9.822	10.903	10.875	10.889	2.5016	9.820	10.930	10.906	10.918	2.5010	120*
5M3B1	5.232	10.808	11.002	10.905	1.3384	-	-	-	-	-	120*
5M3B2	5.520	10.780	10.999	10.890	1.4082	-	-	-	-	-	120*
5M3B3	4.875	10.999	10.723	10.861	1.2279	4.877	10.972	10.745	10.8585	1.2279	120*
5M3B4	4.975	10.900	10.878	10.889	1.2655	-	-	-	-	-	120*
5M3B5	5.532	10.819	10.834	10.827	1.3885	5.551	10.900	10.799	10.8495	1.3878	120*
10M1A1	10.551	11.117	11.025	11.071	2.8481	10.567	11.131	11.029	11.08	2.8470	120*
10M1A2	10.380	11.065	11.043	11.054	2.8267	10.446	11.094	11.053	11.0735	2.8251	120*
10M1A3	10.311	10.994	11.021	11.008	2.7800	10.396	11.033	11.049	11.041	2.7781	120*
10M1A4	10.149	10.800	10.959	10.880	2.6699	10.230	10.977	10.827	10.902	2.6687	120*
10M1A5	10.088	10.945	10.881	10.913	2.6460	10.102	10.958	10.881	10.9195	2.6448	120*
10M1B1	5.268	10.902	11.049	10.976	1.4064	5.327	10.914	11.064	10.989	1.4043	120*
10M1B2	4.892	10.851	11.051	10.951	1.2967	4.943	10.914	11.034	10.974	1.2947	120*
10M1B3	4.950	10.835	10.977	10.906	1.3009	5.019	10.847	10.997	10.922	1.2996	120*
10M1B4	5.300	10.912	10.890	10.901	1.3942	5.373	10.945	10.899	10.922	1.3932	120*
10M1B5	6.365	10.836	10.811	10.824	1.6383	6.443	10.862	10.837	10.8495	1.6374	120*
5V1A1	9.982	11.311	11.100	11.206	2.8099	-	-	-	-	-	120*
5V1A2	9.813	10.911	11.243	11.077	2.6551	-	-	-	-	-	120*
5V1A3	9.566	10.923	11.243	11.083	2.6499	-	-	-	-	-	120*
5V1A4	10.000	11.181	11.254	11.218	2.8184	-	-	-	-	-	120*
5V1A5	9.695	11.465	11.562	11.514	2.8399	-	-	-	-	-	120*
5V1B1	5.402	11.189	11.092	11.141	1.5062	-	-	-	-	-	120*

	Before Heating					After Heating					
Sample	l (mm)	d_1 (mm)	d_2 (mm)	d_{avg} (mm)	m (g)	l (mm)	d_1 (mm)	d_2 (mm)	d_{avg} (mm)	m (g)	Duration (min)
5V1B2	5.312	11.010	10.951	10.981	1.4456	-	-	-	-	-	120*
5V1B3	4.855	11.285	11.159	11.222	1.3676	4.869	11.212	11.239	11.2255	1.3155	120*
5V1B4	5.093	11.091	11.269	11.180	1.4250	-	-	-	-	-	120*
5V1B5	5.159	11.105	11.606	11.356	1.4659	-	-	-	-	-	120*
5V2B1	5.473	11.246	11.354	11.300	1.5643	5.473	11.220	11.353	11.2865	1.5641	30
5V2B2	5.064	11.319	11.381	11.350	1.4677	5.069	11.310	11.448	11.379	1.4666	30
5V2B3	4.948	11.025	11.226	11.126	1.3638	4.941	10.962	11.253	11.1075	1.3626	120
5V2B4	5.117	11.129	11.038	11.084	1.4356	5.115	11.064	11.069	11.0665	1.4347	120
5V2B5	4.888	11.282	11.009	11.146	1.3695	4.889	11.291	10.999	11.145	1.3682	30
5VH2B1	4.991	10.818	10.891	10.855	1.2869	5.011	10.872	10.834	10.853	1.2871	120
5VH2B2	5.293	10.773	10.665	10.719	1.3368	5.292	10.741	10.724	10.7325	1.3365	120
5VH2B3	4.886	10.950	10.811	10.881	1.2558	4.860	10.950	10.803	10.8765	1.2541	30
5VH2B4	4.791	10.912	10.775	10.844	1.2259	4.810	10.886	10.782	10.834	1.2251	30
5VH2B5	4.673	10.607	10.603	10.605	1.1160	4.632	10.609	10.603	10.606	1.1134	30
5VH2B6	5.089	10.641	10.612	10.627	1.2523	5.088	10.634	10.606	10.62	1.2516	120
5VH2B7	5.638	10.640	10.611	10.626	1.3805	5.633	10.649	10.661	10.6551	1.3798	30
5VH2B8	5.350	10.632	10.618	10.625	1.3199	5.345	10.616	10.632	10.624	1.3197	120
7.5V1A1	10.057	10.830	10.894	10.862	2.7915	-	-	-	-	-	120*
7.5V1A2	9.925	10.951	10.793	10.872	2.7300	-	-	-	-	-	120*
7.5V1A3	9.890	11.092	11.099	11.096	2.8553	-	-	-	-	-	120*
7.5V1A4	9.930	11.135	10.968	11.052	2.8672	-	-	-	-	-	0
7.5V1A5	9.896	11.096	11.024	11.060	2.8442	-	-	-	-	-	0
7.5V1B1	5.114	10.982	10.764	10.873	1.4266	-	-	-	-	-	120*
7.5V1B2	5.188	10.895	11.004	10.950	1.4681	-	-	-	-	-	120*
7.5V1B3	5.105	11.037	10.864	10.951	1.4352	-	-	-	-	-	120*
7.5V1B4	4.948	10.917	11.091	11.004	1.4123	4.954	10.915	11.098	11.0065	1.4123	30
7.5V1B5	5.006	10.803	10.947	10.875	1.3937	5.025	10.900	10.942	10.921	1.3933	30
7.5V2B1	5.128	11.315	11.384	11.350	1.5384	5.136	11.286	11.386	11.336	1.5376	30
7.5V2B2	5.033	11.275	11.383	11.329	1.5071	5.036	11.334	11.298	11.316	1.5066	120
7.5V2B3	5.002	11.304	11.322	11.313	1.4988	4.984	11.278	11.371	11.3245	1.4983	120
10V1A1	10.028	11.099	11.212	11.156	3.0170	-	-	-	-	-	0
10V1A2	9.854	11.040	10.944	10.992	2.9106	-	-	-	-	-	0
10V1A3	10.268	10.943	10.871	10.907	2.9452	-	-	-	-	-	0
10V1A4	10.109	11.133	11.174	11.154	3.0450	-	-	-	-	-	0
10V1A5	10.005	11.128	11.174	11.151	3.0418	-	-	-	-	-	0
10V1B1	4.982	11.001	11.208	11.105	1.5015	4.999	11.222	11.015	11.1185	1.4968	30
10V1B2	4.687	10.953	11.082	11.018	1.3851	4.685	10.900	11.101	11.0005	1.3822	30
10V1B3	4.829	10.965	11.218	11.092	1.4340	4.830	10.949	11.198	11.0735	1.4298	30
10V1B4	4.977	11.029	10.984	11.007	1.4569	4.986	11.090	10.870	10.98	1.4540	120
10V1B6	4.800	10.674	10.724	10.699	1.2946	4.807	10.669	10.761	10.715	1.2938	120
10V2B1	5.225	11.158	11.144	11.151	1.5815	5.225	11.180	11.143	11.1615	1.5810	120
25V1B1	5.346	11.677	12.084	11.881	2.2192	5.363	11.713	12.094	11.9035	2.2194	30
25V1B2	5.361	11.844	11.665	11.755	2.1587	5.487	11.890	11.829	11.8595	2.1583	120
25V1B3	5.228	11.675	12.018	11.847	2.1787	5.253	11.760	12.089	11.9245	2.1795	30
25V1B4	5.121	11.869	11.669	11.769	2.1201	5.246	11.787	12.096	11.9415	2.1197	120
25VH2B1	5.081	10.744	10.775	10.760	1.7228	5.074	10.750	10.796	10.773	1.7224	30
25VH2B2	5.203	10.734	10.769	10.752	1.7638	5.176	10.737	10.769	10.753	1.7635	120
25VH2B3	5.190	10.751	10.759	10.755	1.7620	5.192	10.760	10.756	10.758	1.7615	30
25VH2B4	5.172	10.648	10.694	10.671	1.7355	5.173	10.694	10.659	10.6765	1.7348	120
50V1B1	5.742	11.489	11.702	11.596	2.9105	5.967	12.005	11.852	11.9285	2.8986	30
50V1B2	5.259	11.870	11.826	11.848	2.7989	5.609	12.245	12.145	12.195	2.7983	120
50V1B3	5.265	11.652	11.479	11.566	2.6871	5.390	11.827	11.710	11.7685	2.6879	30
50V1B4	5.281	11.880	11.651	11.766	2.7769	5.596	12.178	12.159	12.1685	2.7769	120
50V1B5	5.034	11.527	11.785	11.656	2.6032	5.037	11.504	11.783	11.6435	2.6033	5
50VH2B1	5.977	10.828	10.791	10.810	2.6579	6.018	10.858	10.919	10.8885	2.6569	30
50VH2B2	6.072	10.908	10.882	10.895	2.6963	6.150	10.975	10.873	10.924	2.6963	120
50VH2B3	4.823	10.895	10.967	10.931	2.1797	4.861	11.031	10.963	10.997	2.1802	30
50VH2B4	5.033	10.927	10.896	10.912	2.2626	5.091	11.051	11.045	11.048	2.2626	120

* Heated in vacuum drying oven

LIST OF REFERENCES

[1] J. Kaneshiro, "New technology holds promise of greater lethality," U.S. Army, April 12, 2012. [Online]. Available: https://www.army.mil/article/77589/new_technology_holds_promise_of_greater_lethality.

[2] A. Gökçe and F. Fındık, "Mechanical and physical properties of sintered aluminum powders," *J. Achiev. Mater. Manuf. Eng.*, vol. 30, no. 2, pp. 157–164, Oct. 2008. [Online]. Available: http://citeseerx.ist.psu.edu/viewdoc/download?doi=10.1.1.563.1942&rep=rep1&type=pdf

[3] J. Kline and J. P. Hooper, "The effect of annealing on the impact fragmentation of a pure aluminum reactive material," *J. Appl. Phys.*, vol. 125, no. 205901, pp. 1–9, May 2019. [Online]. doi: https://doi.org/10.1063/1.5094444

[4] D. A. Kotei, "Aluminum reactive material warhead casings," M.S. thesis, Dept. of Mech. and Aerosp. Eng., NPS, Monterey, CA, USA, 2018. [Online]. Available: http://hdl.handle.net/10945/61209

[5] *ASM Handbook* (Vol. 2 – Properties and Selection: Nonferrous Alloys and Special-Purpose Materials), 10th ed. ASM International, 1990.

[6] Ted Pella, Inc., "Hardness tables," Accessed May 13, 2020. [Online]. Available: https://www.tedpella.com/company_html/hardness.htm

[7] Valimet Inc., *Aluminum H-series data sheet*, 2017. Accessed Mar. 21, 2020. [Online]. Available: https://valimet.com/wp-content/uploads/2017/08/Aluminum-H-Series-Data-Sheet-.pdf

[8] Millipore Sigma, "Tin 520373." Accessed Mar. 21, 2020. [Online]. Available: https://www.sigmaaldrich.com/catalog/product/aldrich/520373?lang=en&region=US

[9] R. Singh, "Working with metals," in *Applied Welding Engineering*, 2nd ed. Elsevier, 2016, pp. 99–102.

[10] Tyne and Wear Oils, "Greases explained," April 12, 2019. [Online]. Available: https://twoils.co.uk/greases-explained.html.

[11] L. N. Y. Wong and D. Li, "The Brazilian disc test for rock mechanics applications: review and new insights," *Rock Mech. Rock Eng.*, vol. 46, pp. 269–287, May 2012. [Online]. doi: https://doi.org/10.1007/s00603-012-0257-7

[12] *Standard Test Method of Fracture Toughness*, ASTM Standard E1820-01, 2001. doi: https://doi.org/10.1520/E1820-01

[13] M. Tang and J. P. Hooper, “Impact fragmentation of a brittle metal compact,” *J. Appl. Phys.*, vol. 123, no. 17, May 2018. [Online]. doi: https://doi.org/10.1063/1.5026711

[14] AZO Materials, “Different types of SEM imaging – BSE and secondary electron imaging,” Aug. 4, 2017. [Online]. Available: https://www.azom.com/article.aspx?ArticleID=14309

[15] P. S. Liu and G. F. Chen, “Characterization methods: basic factors,” in *Porous Materials*, 1st ed. Oxford, UK: Elsevier, 2014.

[16] *Standard Test Method for Splitting Tensile Strength of Intact Rock Core Specimens,* ASTM Standard D3967-08, 2008. doi: https://doi.org/10.1520/D3967-08

[17] P. Guo and X. Su, “Shear strength, interparticle locking, and dilatancy of granular materials,” *Can. Geotech. J.*, vol. 44, no. 5, pp. 579–591, Jun. 2007. [Online]. doi: https://doi.org/10.1139/t07-010

INITIAL DISTRIBUTION LIST

1. Defense Technical Information Center
   Ft. Belvoir, Virginia

2. Dudley Knox Library
   Naval Postgraduate School
   Monterey, California